CONSTRAINING DARK MATTER WITH STRONG GRAVITATIONAL LENSING

Simona Vegetti

Outline

- History and theory of gravitational lensing
- Observational evidence of dark matter from gravitational lensing
- Dark matter on scales of 1 - 10 kpc
  - how much dark matter is there?
  - how is dark matter distributed?
  - do we really need dark matter?
- Dark matter on scales of 10 - 100 kpc
  - how is dark matter distributed in the outer regions of haloes?

Yesterday

- Dark matter on scales smaller than 1 kpc
  - measuring the amount of substructure

Today

WHY?

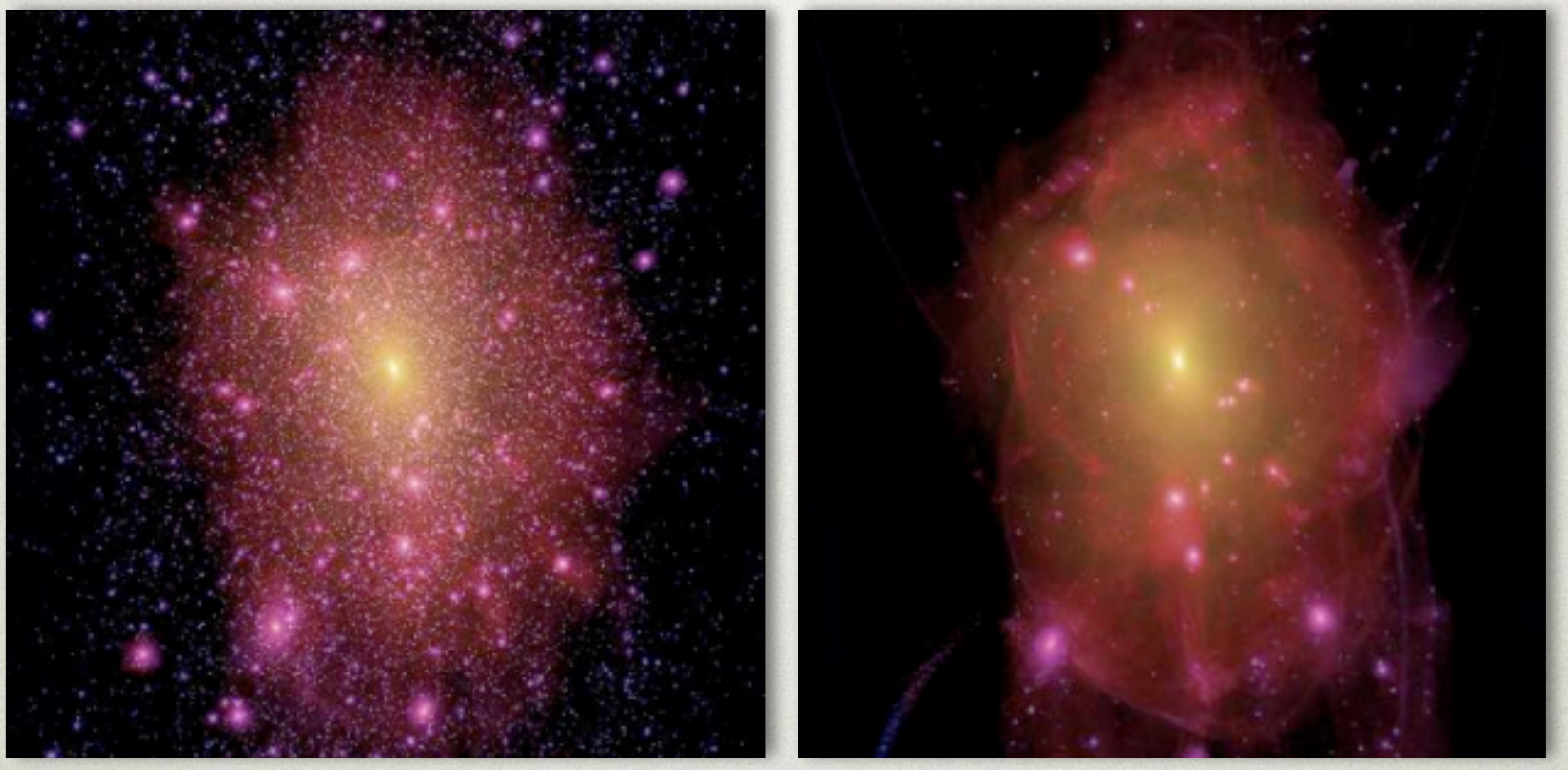

The amount of substructure strongly depends on the nature of dark matter

Where are the satellites?

Mass Function

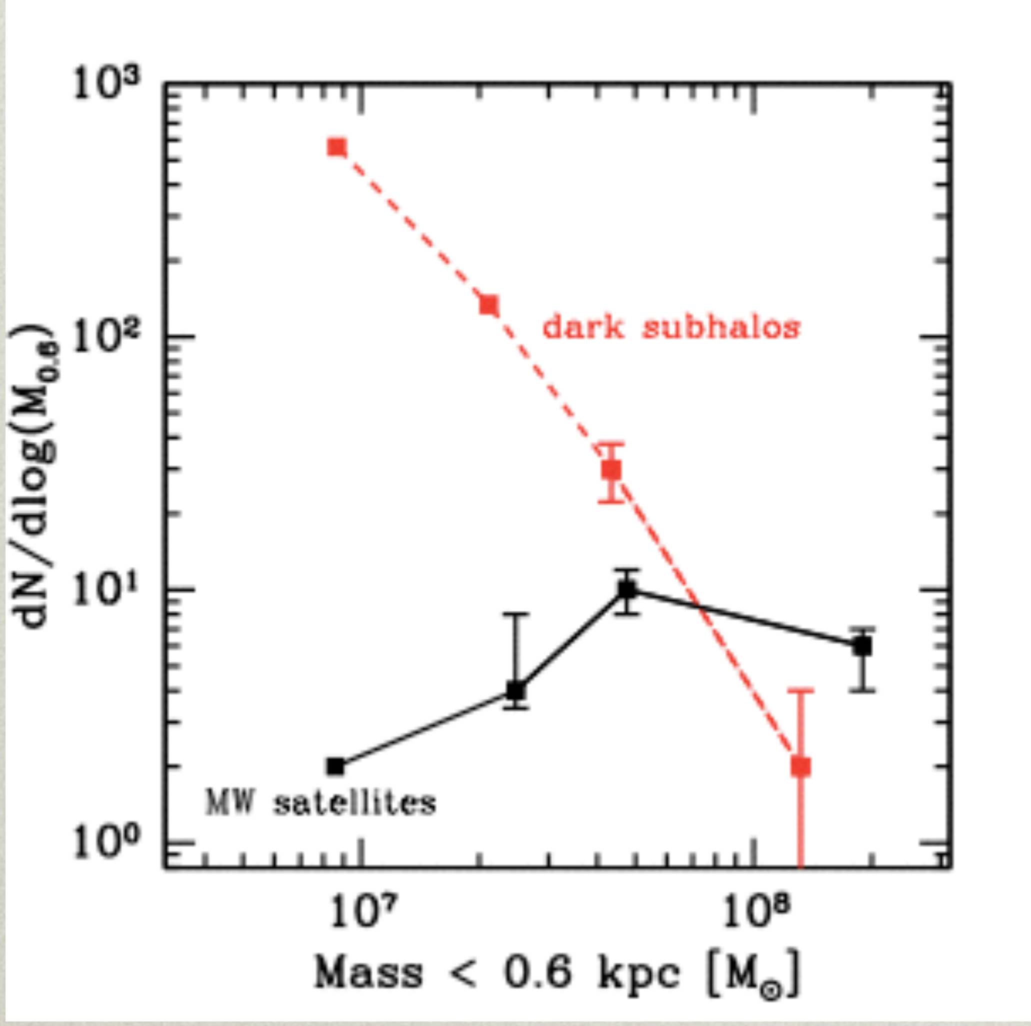

$dN/dm \propto m^{-1.0}$ $dN/dm \propto m^{-1.9}$

Three possible solutions:

- Kill them
- Hide them
- Ignore them

How do we probe the small scales beyond the Local Universe and independently from baryons?

Using strong gravitational lensing!

- Independent of the baryonic content
- Independent of the dynamical state of the system
- Only way to probe small satellites at high redshift

Gravitational Lensing

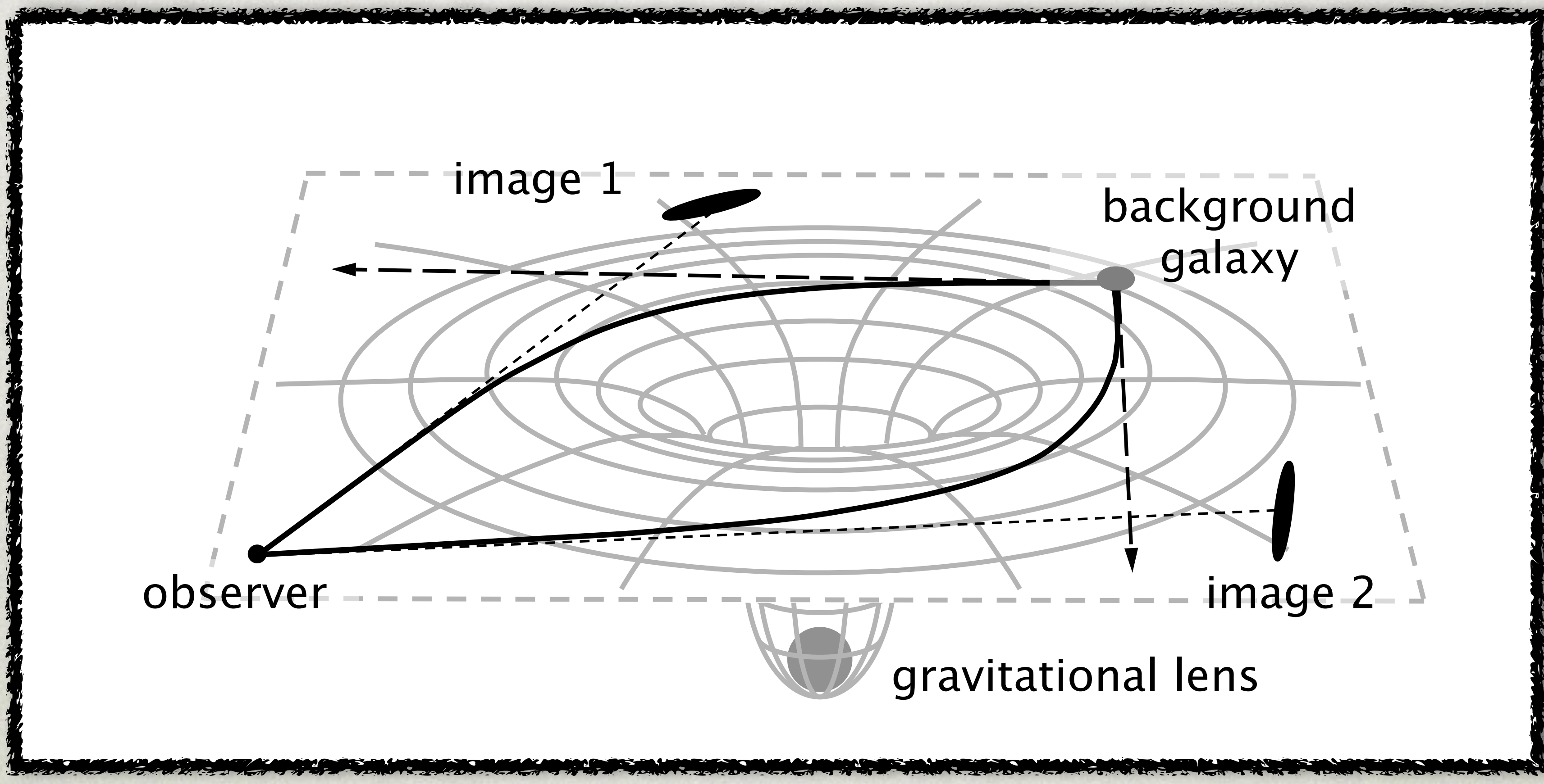

$$\mathbf{y} = \mathbf{x} - \alpha(\mathbf{x}) \qquad \alpha(\mathbf{x}) \propto \int d\mathbf{x}' \int dz \rho(\mathbf{x}', z) \frac{\mathbf{x} - \mathbf{x}'}{|\mathbf{x} - \mathbf{x}'|^2}$$

Substructure Lensing

Strong lensing dark matter substructure probe	Dark matter mass function moment dependence	Dark matter substructure mass range sensitivity	Sensitivity to area around each lensed image	Sensitivity to the internal structure of substructure	Main observational challenges
Time delays	$\left(\langle m^2\rangle/\langle m\rangle\right)^2$	High mass ($<10^9$ M_{sun})	Long-range	Little	High time domain precision
Relative positions	$\left(\langle m^2\rangle/\langle m\rangle\right)^{3/2}$	Intermediate to high mass	Intermediate	Modest	High astrometric precision; lens modeling
Relative fluxes	$\left(\langle m^2\rangle/\langle m\rangle\right)$	Full mass range	Quasi-local	Sensitive	Microlensing; lens modeling

Time Delays

$$\tau(\theta) \propto \left(\frac{1}{2}(\theta-\beta)^2 - \psi(\theta)\right)$$

$$\nabla\tau(\theta) = 0$$

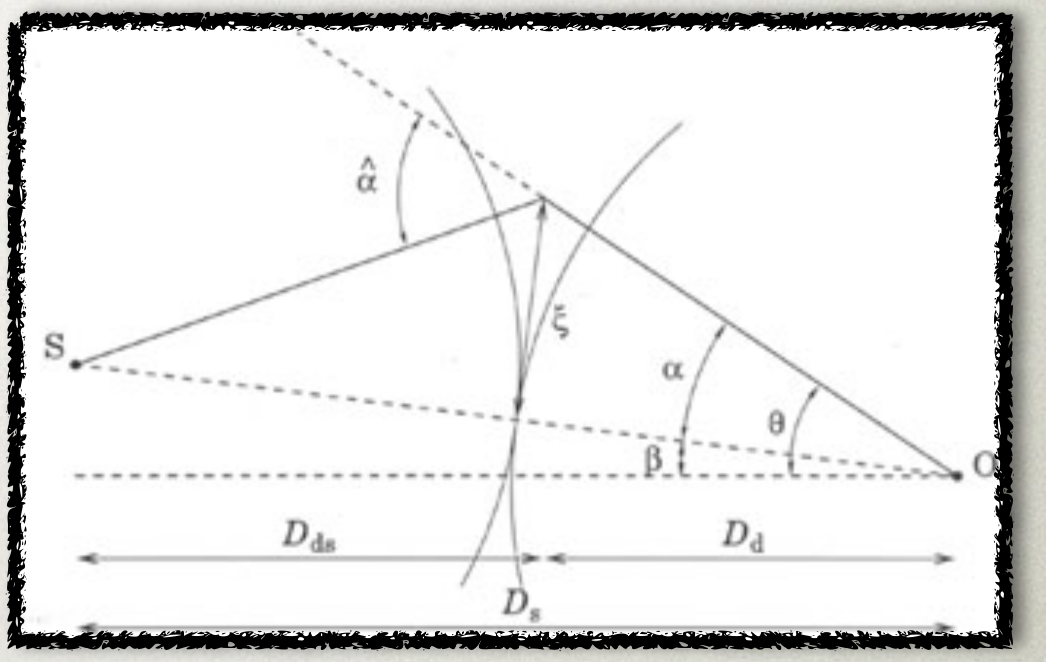

- For a variable source you can measure the differential time delay between two lensed images
- Mass substructure will perturb the projected potential, hence the time delay
- Time delay fluctuations due to substructure are of the order of 1% with a large scatter

Folds & Cusps

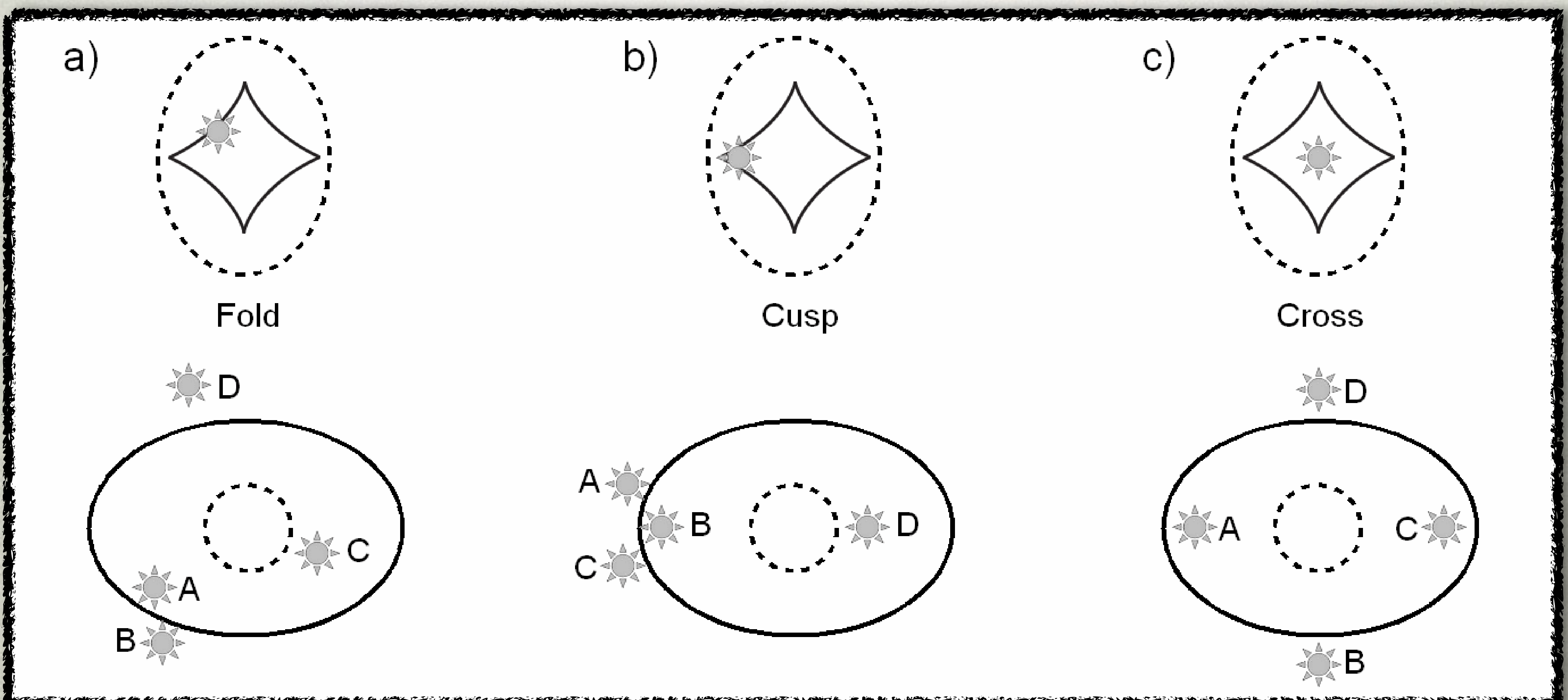

The effect of substructure on time delays is different for the cusp and fold configuration

Time Delays - fold

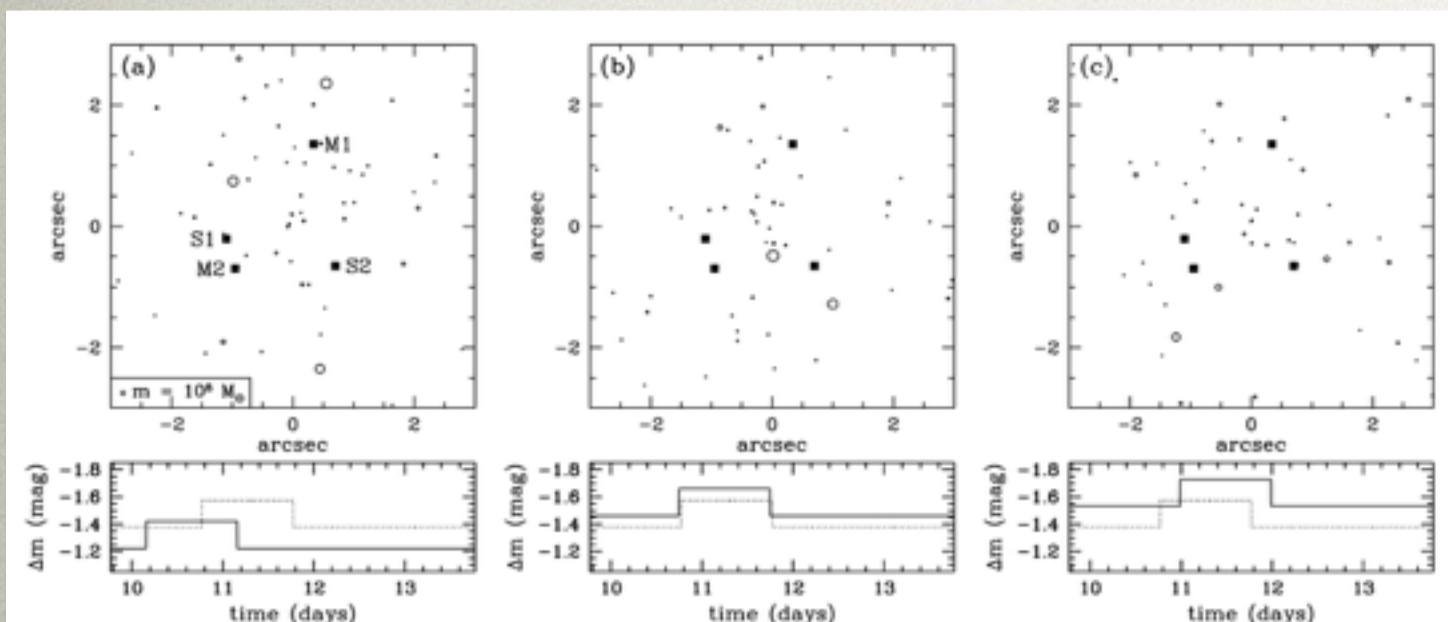

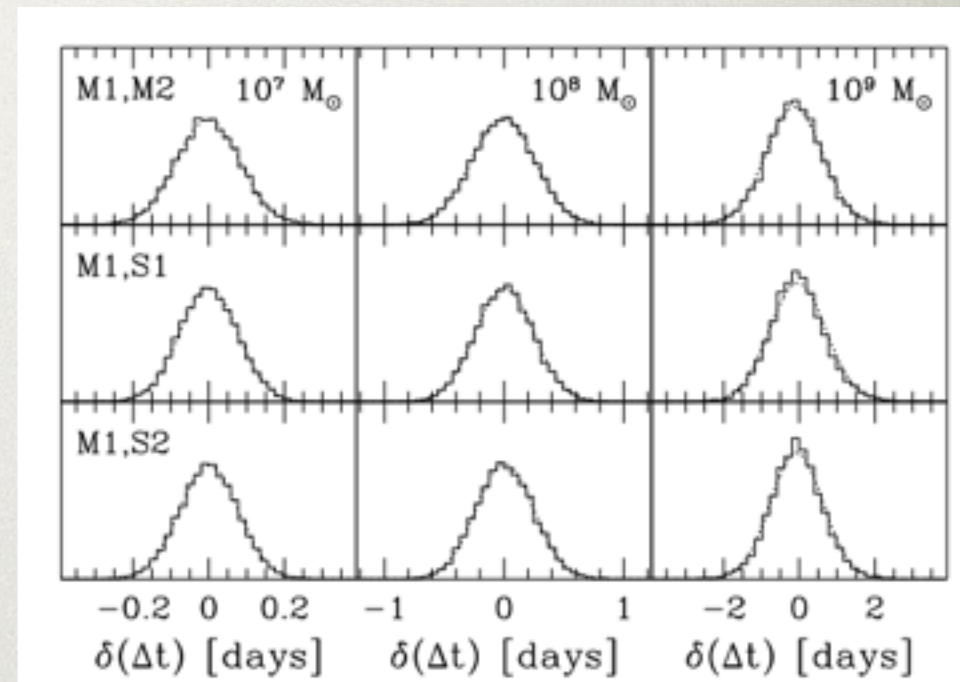

Changes by a % of a day

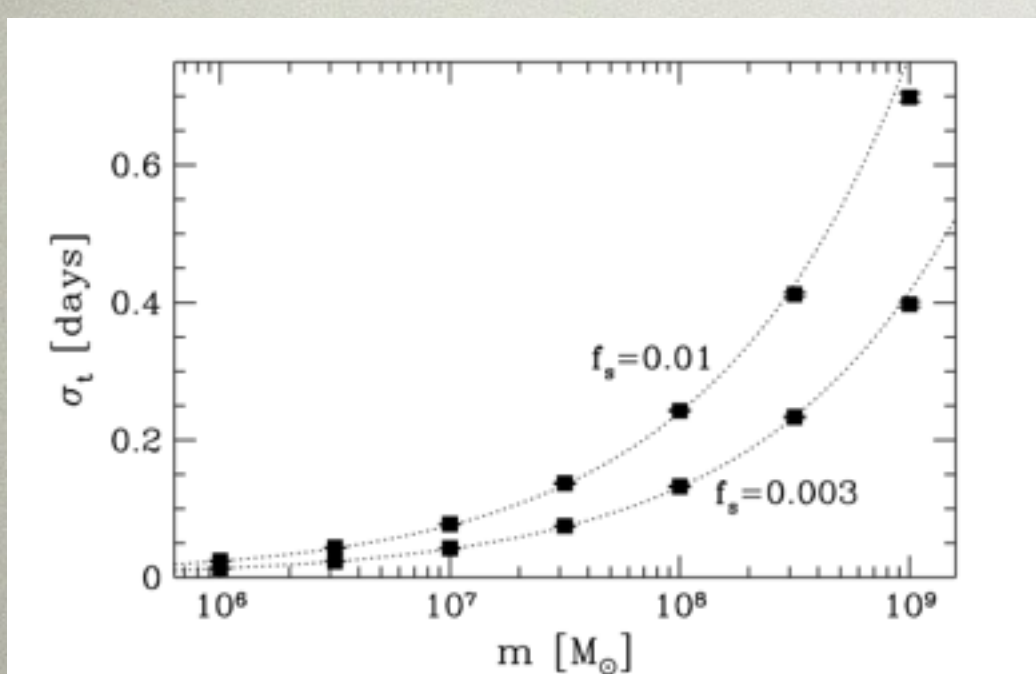

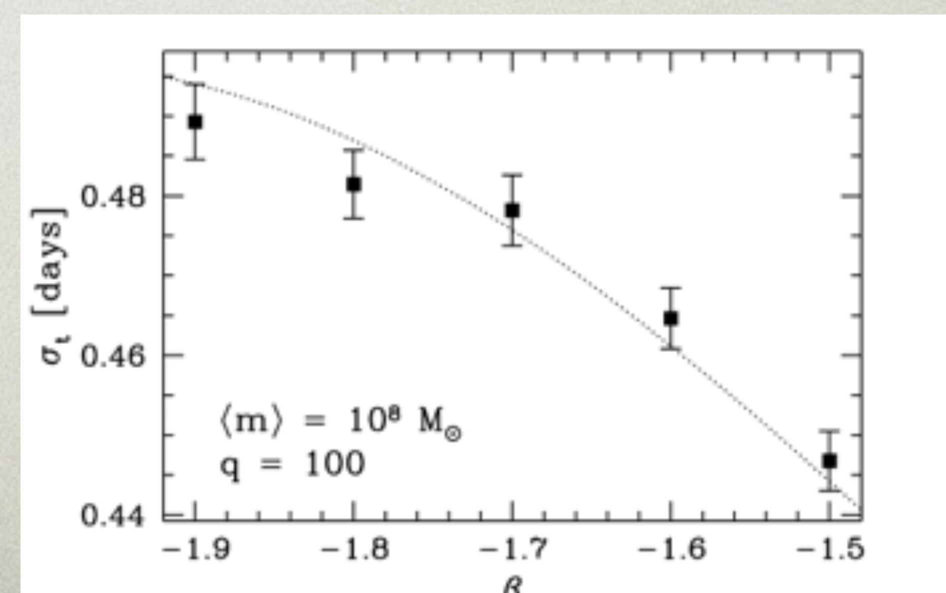

Folds & Cusps

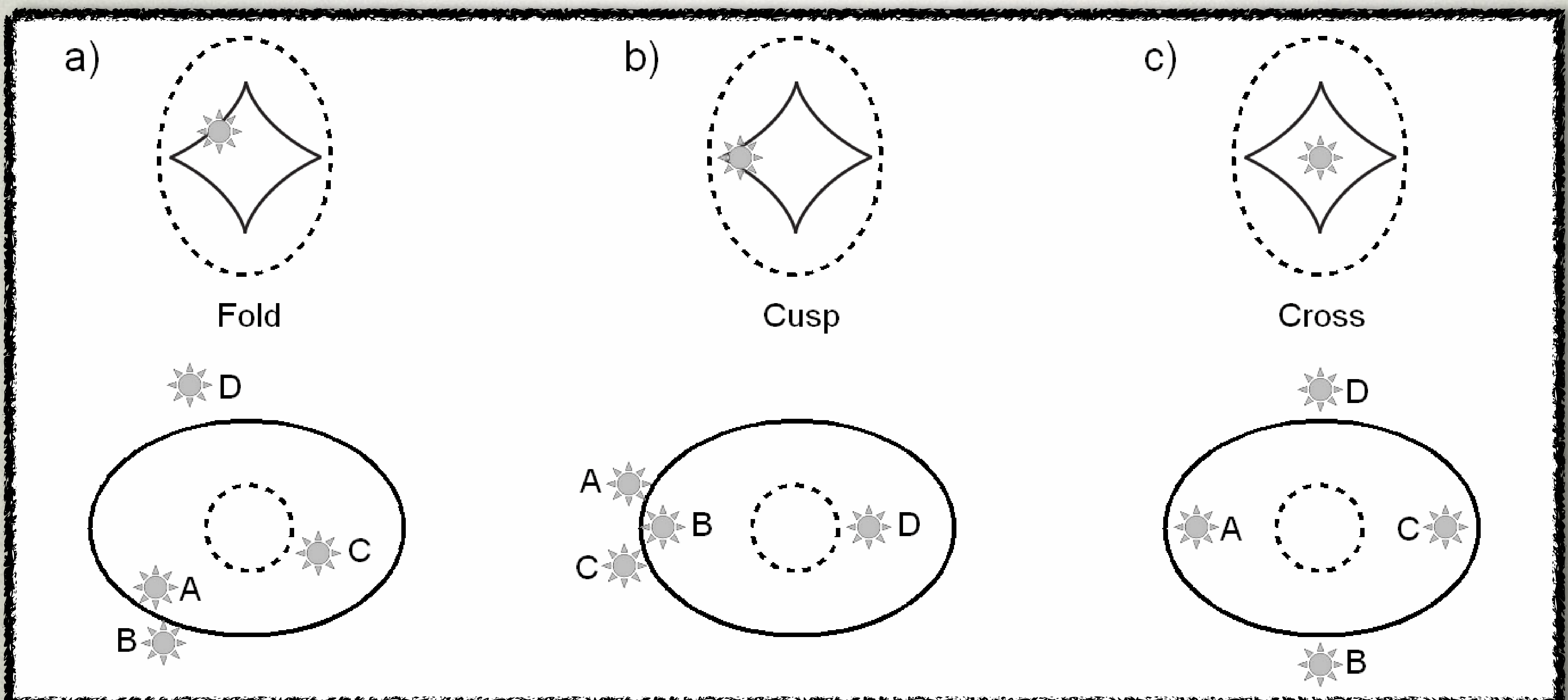

The effect of substructure on time delays is different for the cusp and fold configuration

Time Delays - Cusp

contours of constant
arrival time

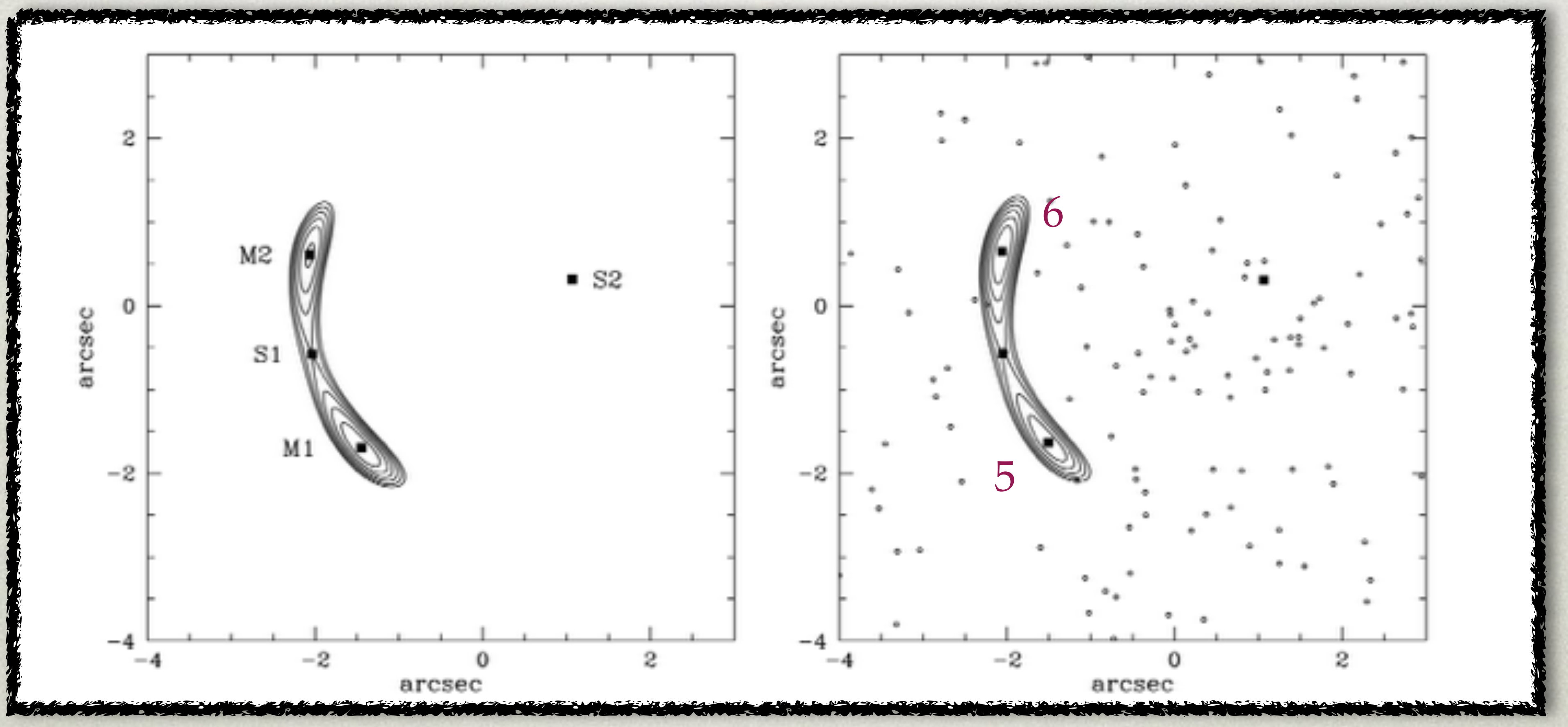

- If the potential is smooth the arrival order is: M1, M2, S1, S2
- The substructure affects the arrival order to: M2, M1, S1, S2 for 27% of the realizations

Flux Ratio Anomalies

Smooth lens modeling can fit the image positions well, but fail to reproduce the relative fluxes

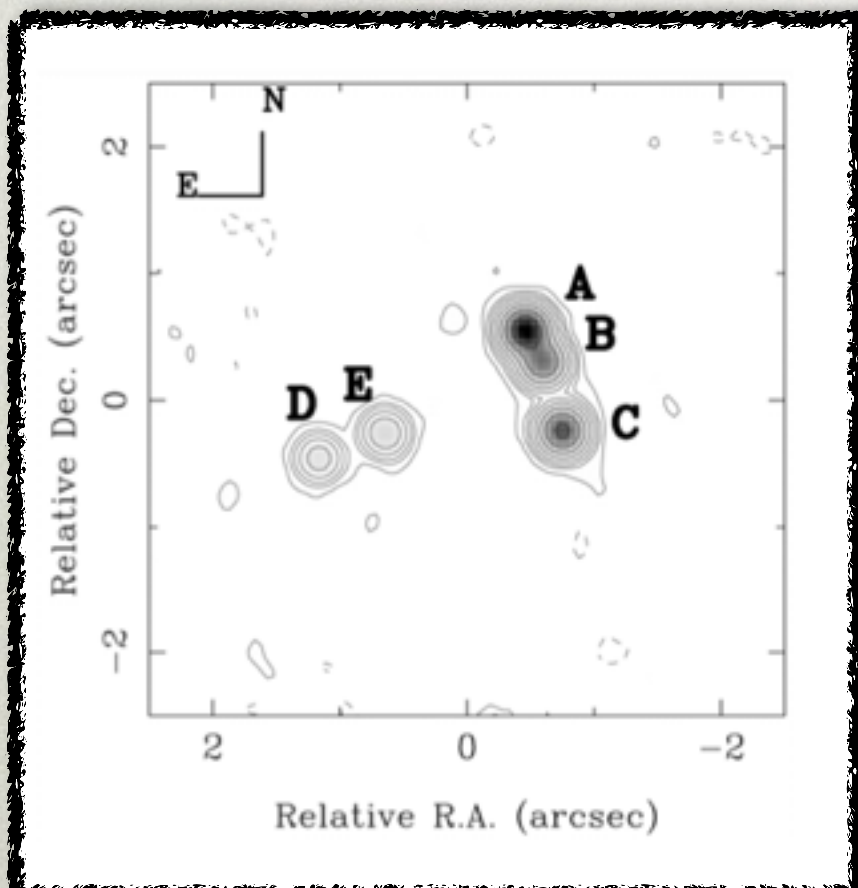

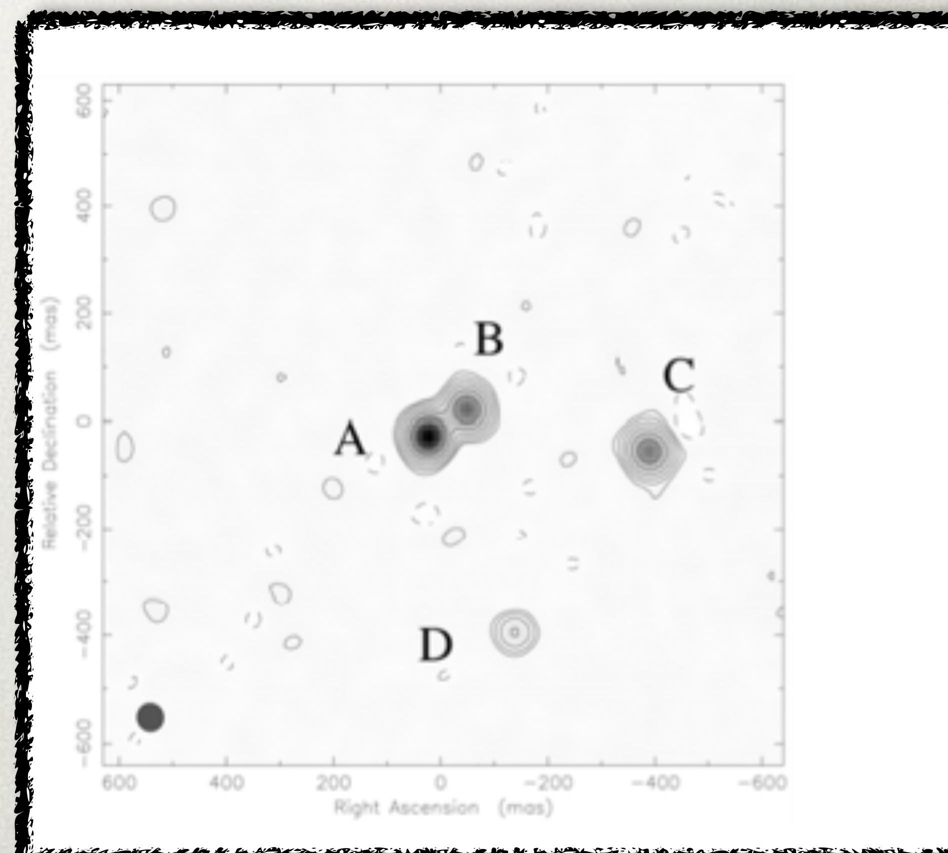

Smooth models produces images B which are as bright as A

Smooth models produces images B which are as bright as A

Flux Ratio Anomalies

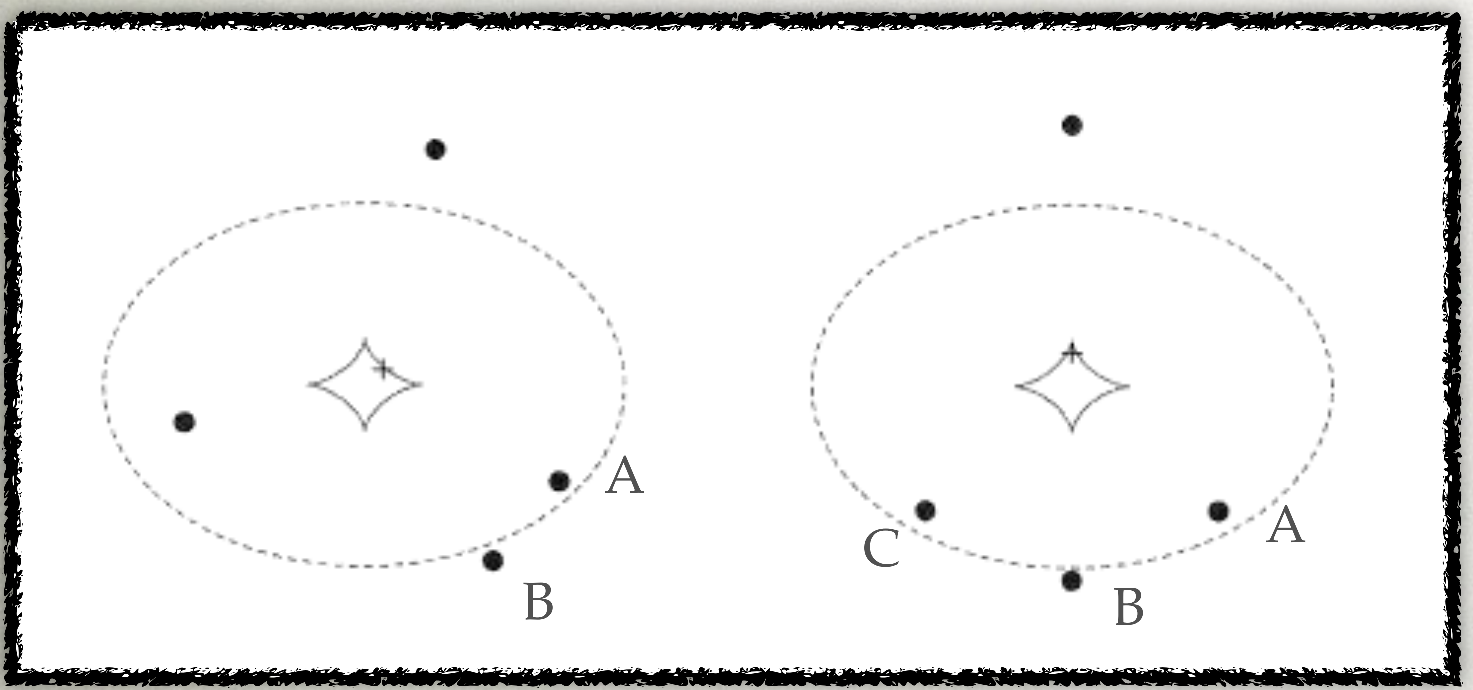

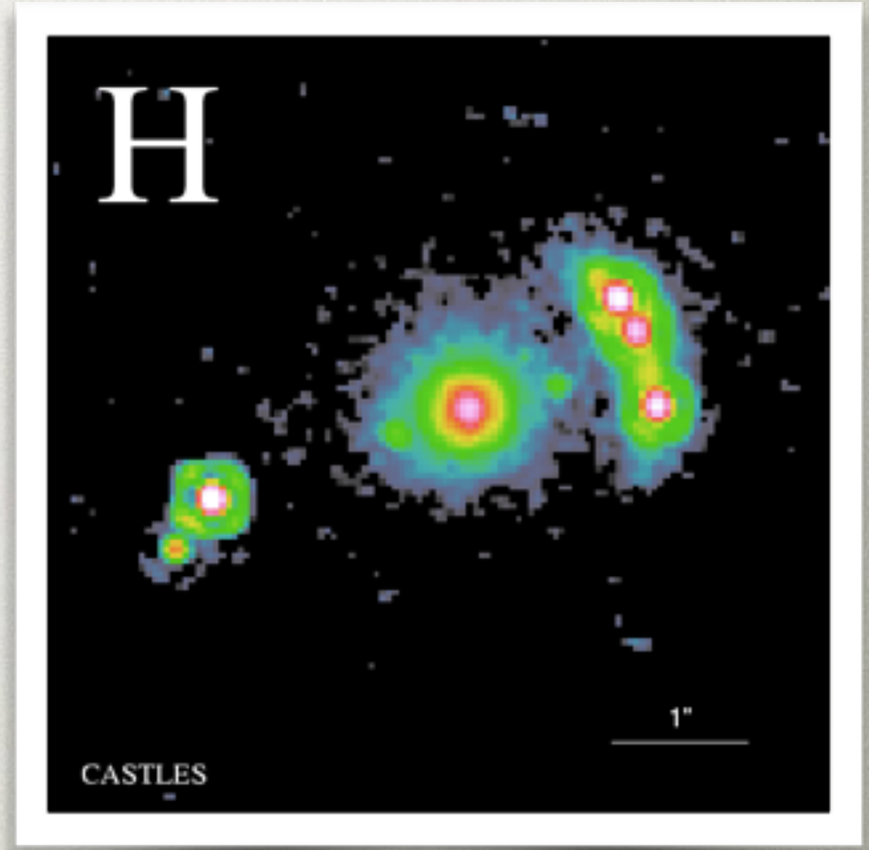

$$R_{\rm fold} = \frac{\mu_A + \mu_B}{|\mu_A| + |\mu_B|} \to 0$$

$$R_{\rm cusp} = \frac{\mu_A + \mu_B + \mu_C}{|\mu_A| + |\mu_B| + |\mu_C|} \to 0$$

In the optical and X-ray the quasar emission regions are small enough that the lens fluxes are sensitive to the effect of stars. In the radio the sources are large enough be insensitive to microlensing

Flux Ratio Anomalies

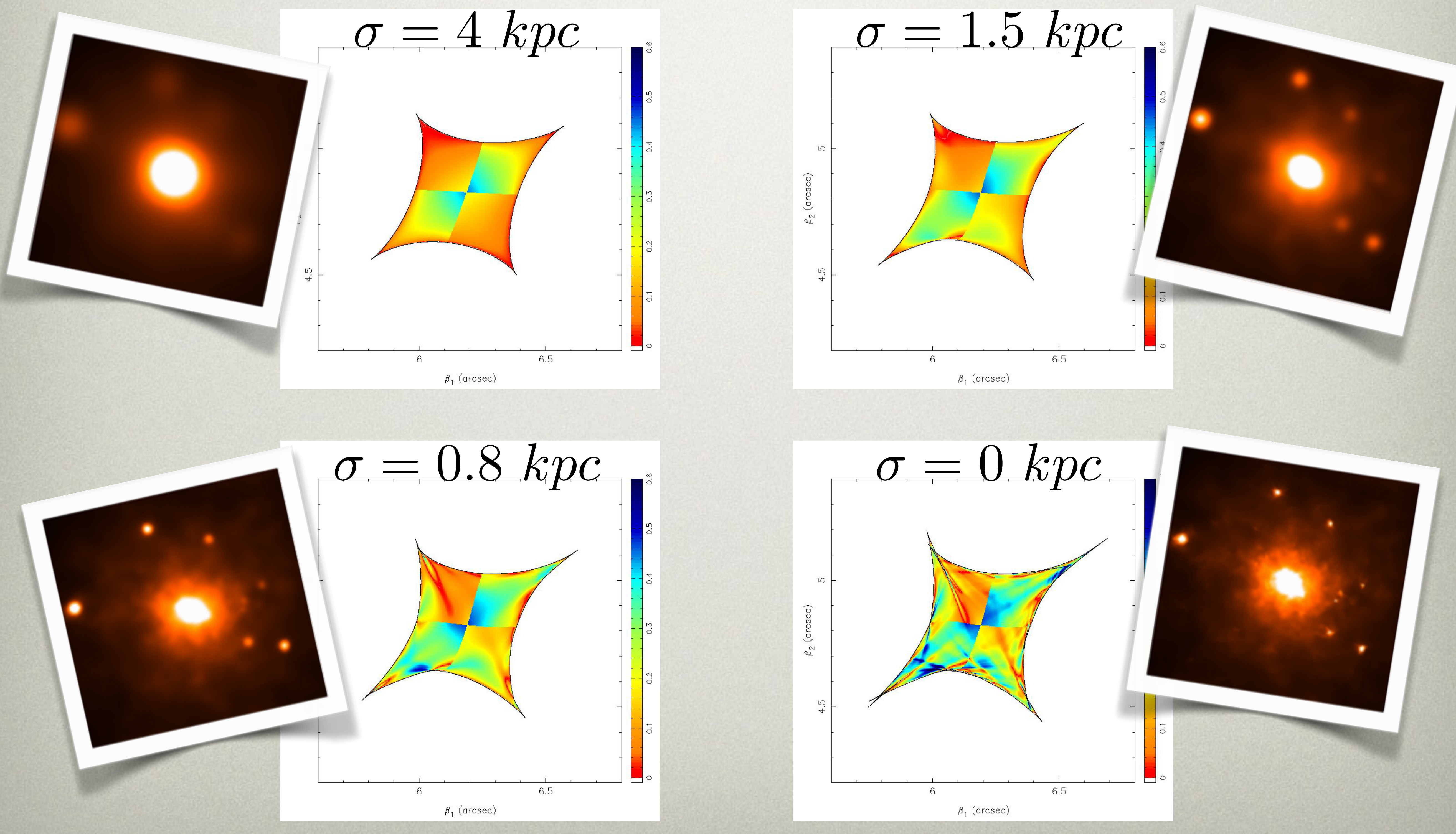

Observed Flux Ratio Anomalies

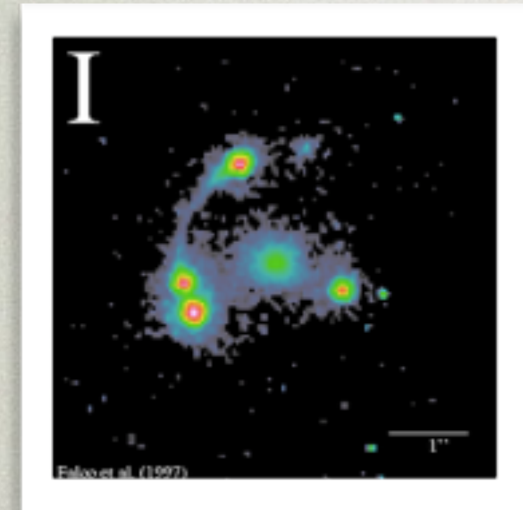

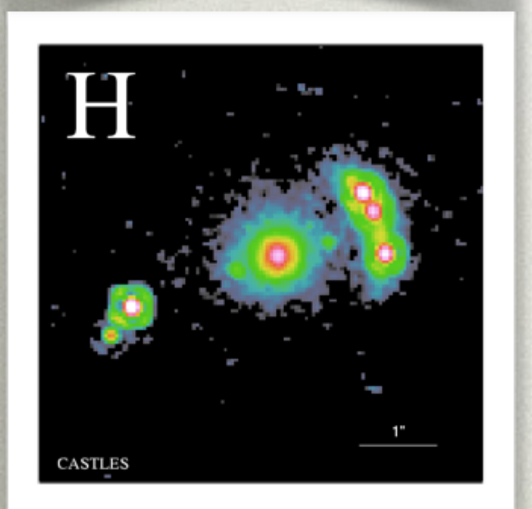

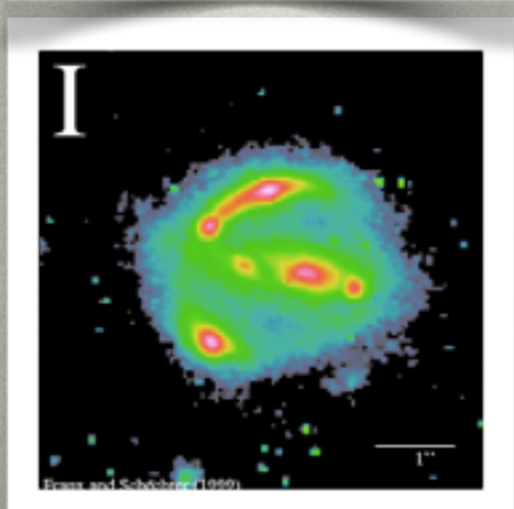

- 6/7 radio loud CLASS lenses show a flux ratio anomaly
- No microlensing, or dust extinction but gravitational origin
- Imply a projected dark matter fraction between 2 and 7 percent
- Because of the mass degeneracy we don't know how this mass is distributed

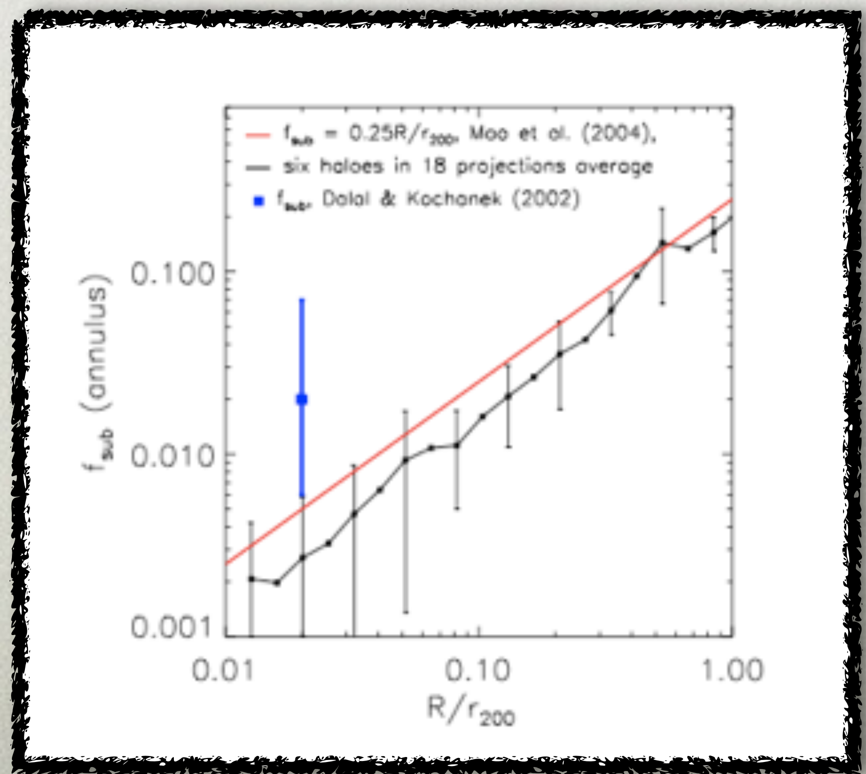

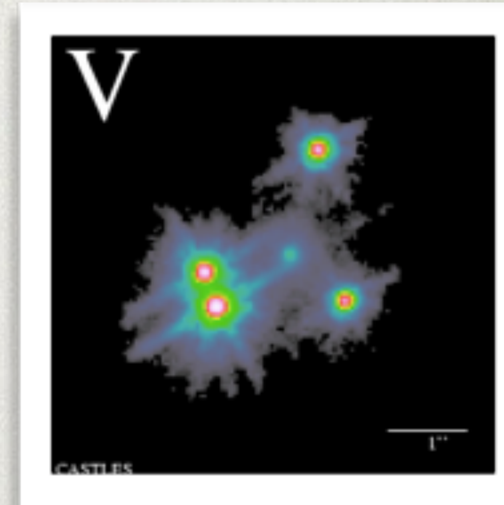

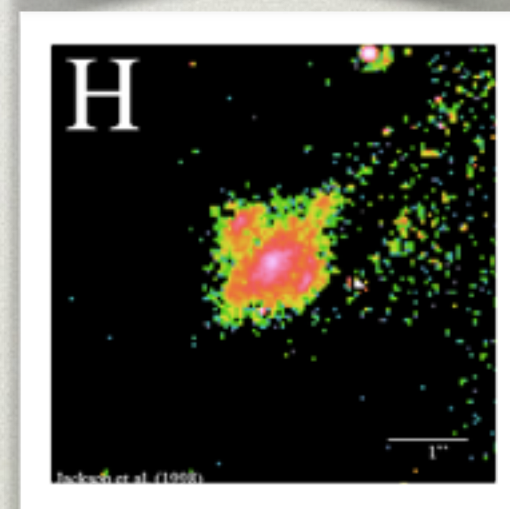

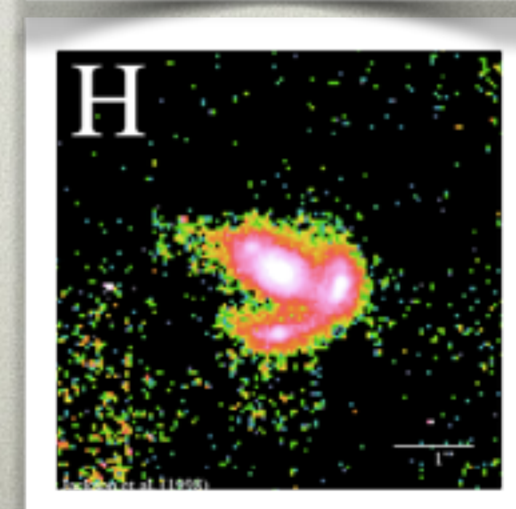

Flux Ratio Anomalies in Simulations

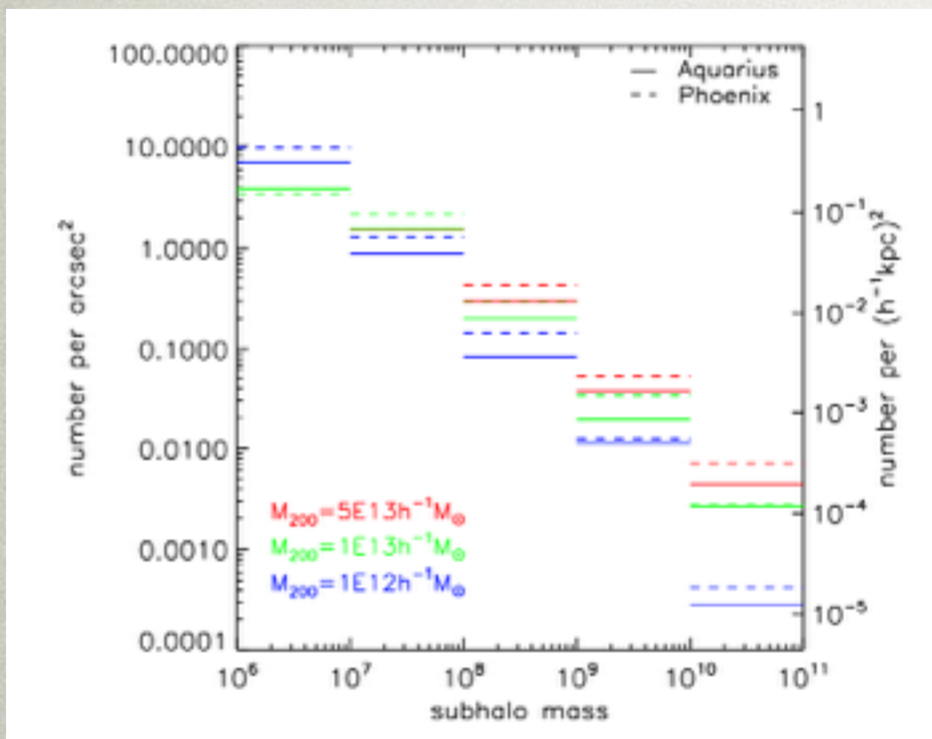

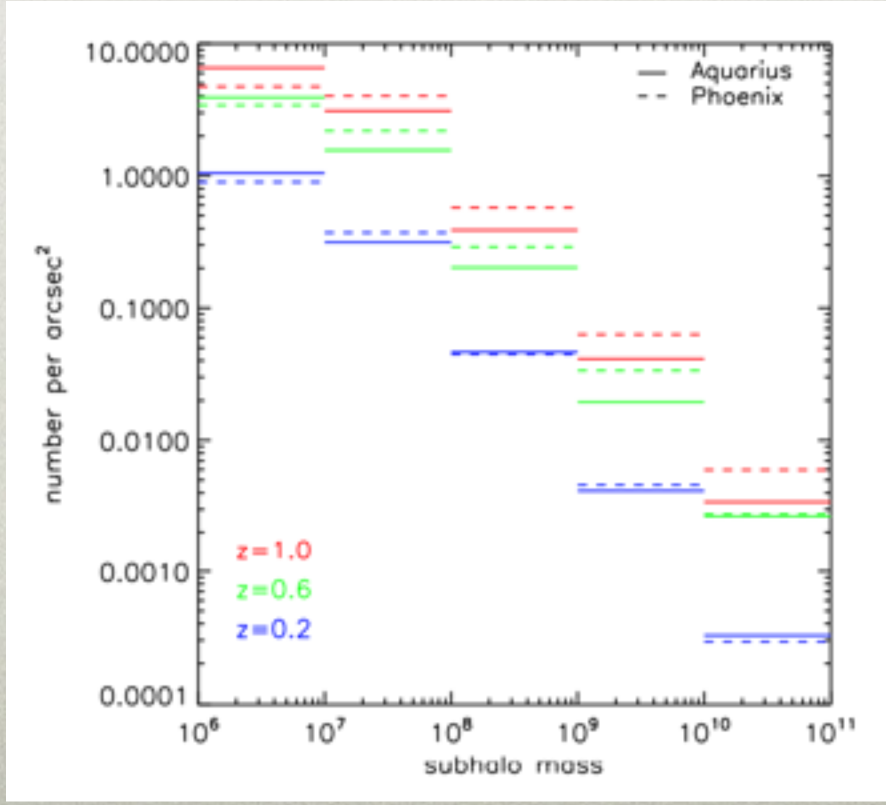

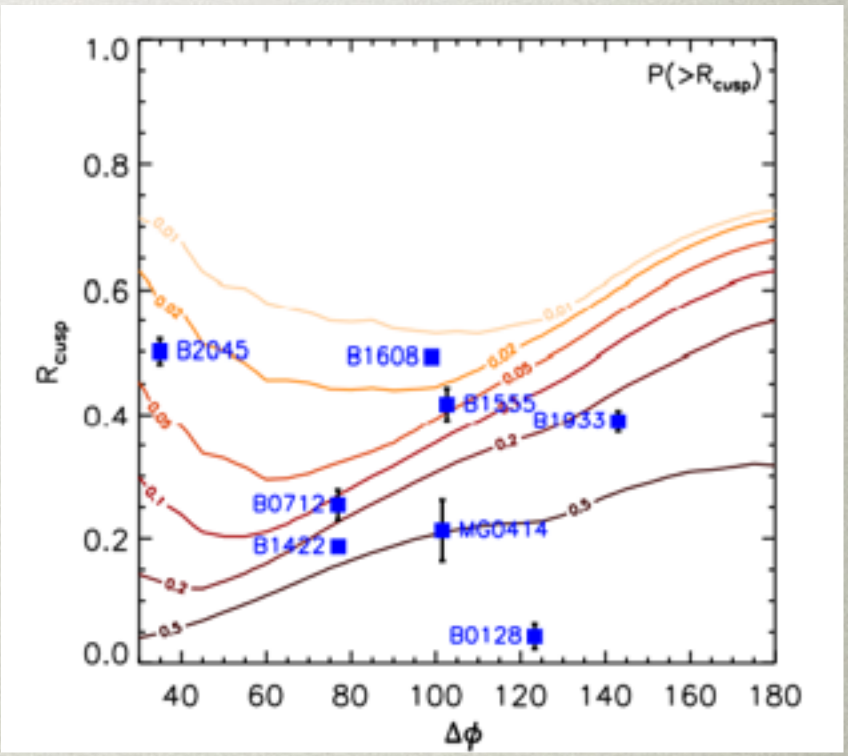

Luminous satellites

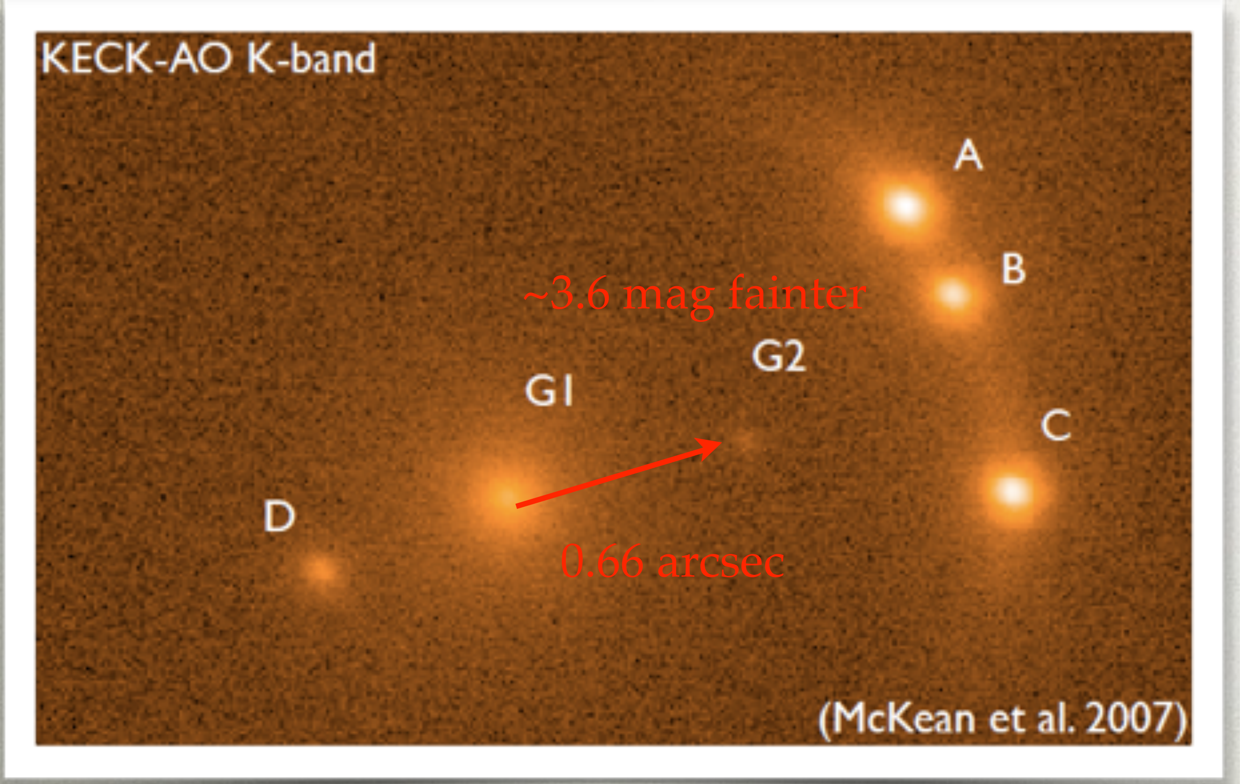

- 3/6 radio loud systems show evidence of a luminous satellite within 5 kpc from the host galaxy
- once these are included in the mass model the flux ratios can be reproduced along side with the images positions
- up to 1% of the host mass is contained in these systems
- 5/22 of all CLASS lenses have a luminous satellite within 5 kpc

- Are such luminous satellite galaxies expected this frequently?

Gravitational Imaging

substructures are detected as magnification anomalies

Compact sources are easy to model

Sensitive to a wide range of masses

degenerate in the mass model

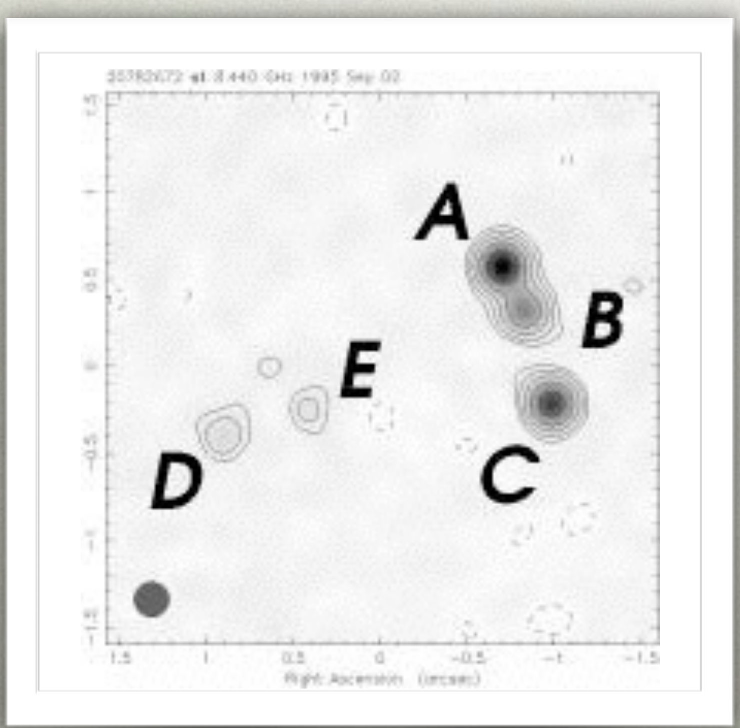

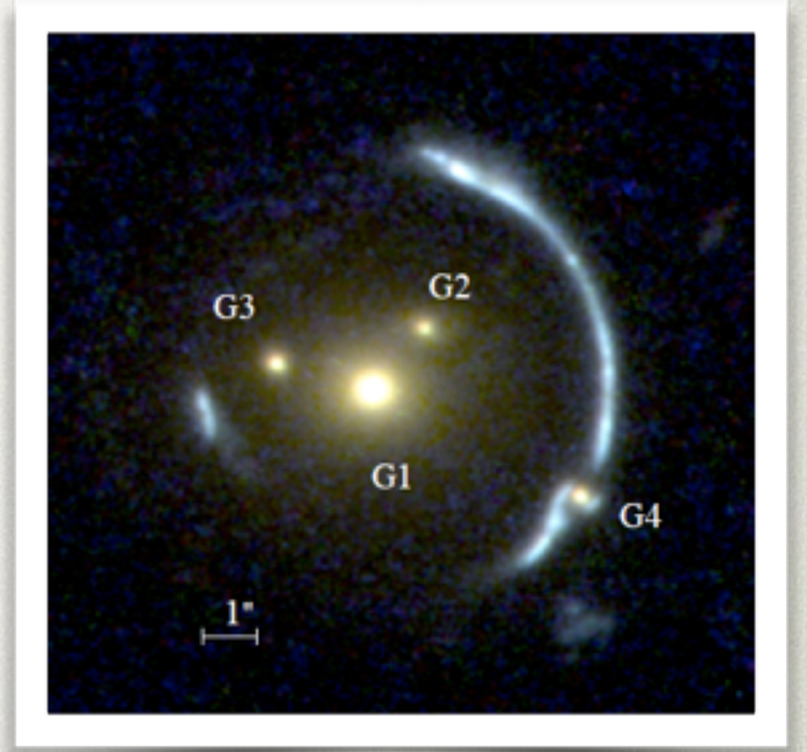

substructures are detected as surface brightness anomalies

need to disentangle structures in the potential from structures in the source

Sensitive to higher masses

NOT degenerate in the mass model

Gravitational Imaging

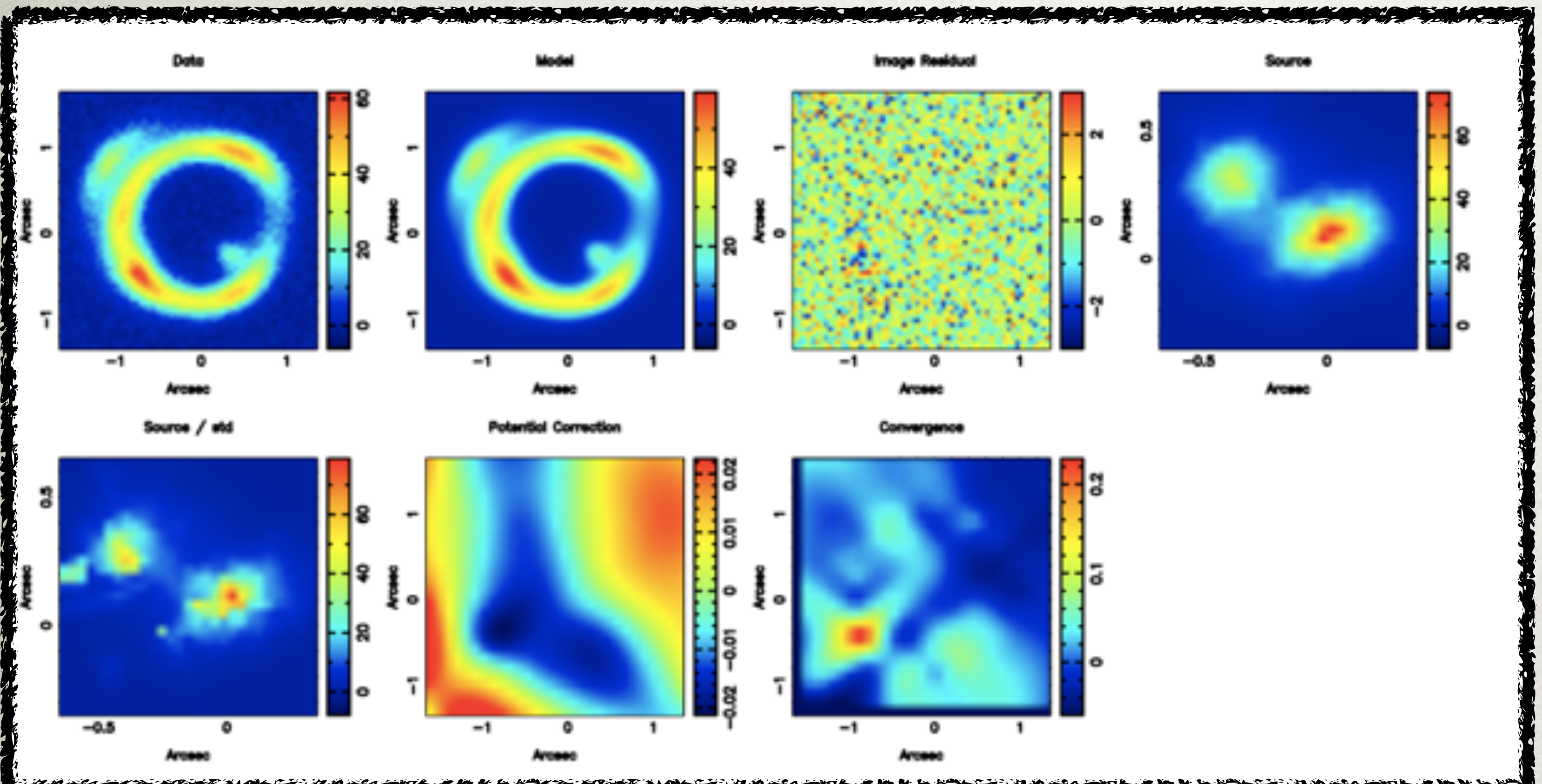

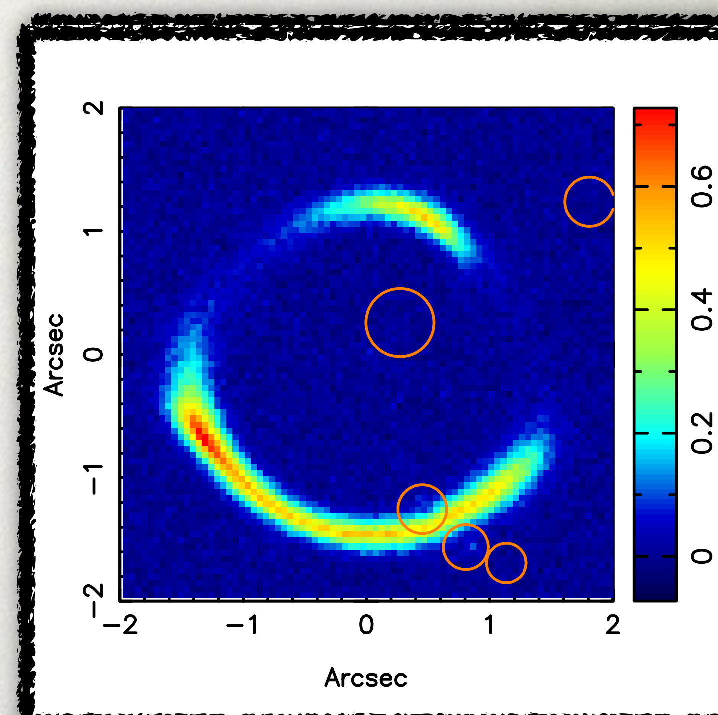

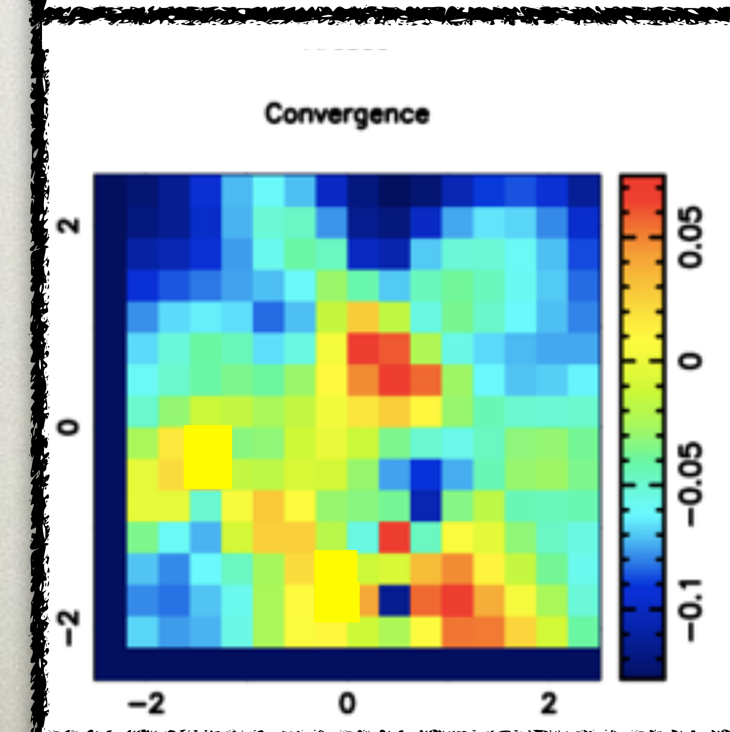

- substructures are responsible of localised surface brightness perturbations and are detected as localised potential corrections

- Any substructure can be detected provided it is mass enough and/or close enough to the Einstein ring

- For each substructure detected its mass can be measured by assuming a mass model or directly from the pixelated corrections in a model independent way

Modeling Procedure

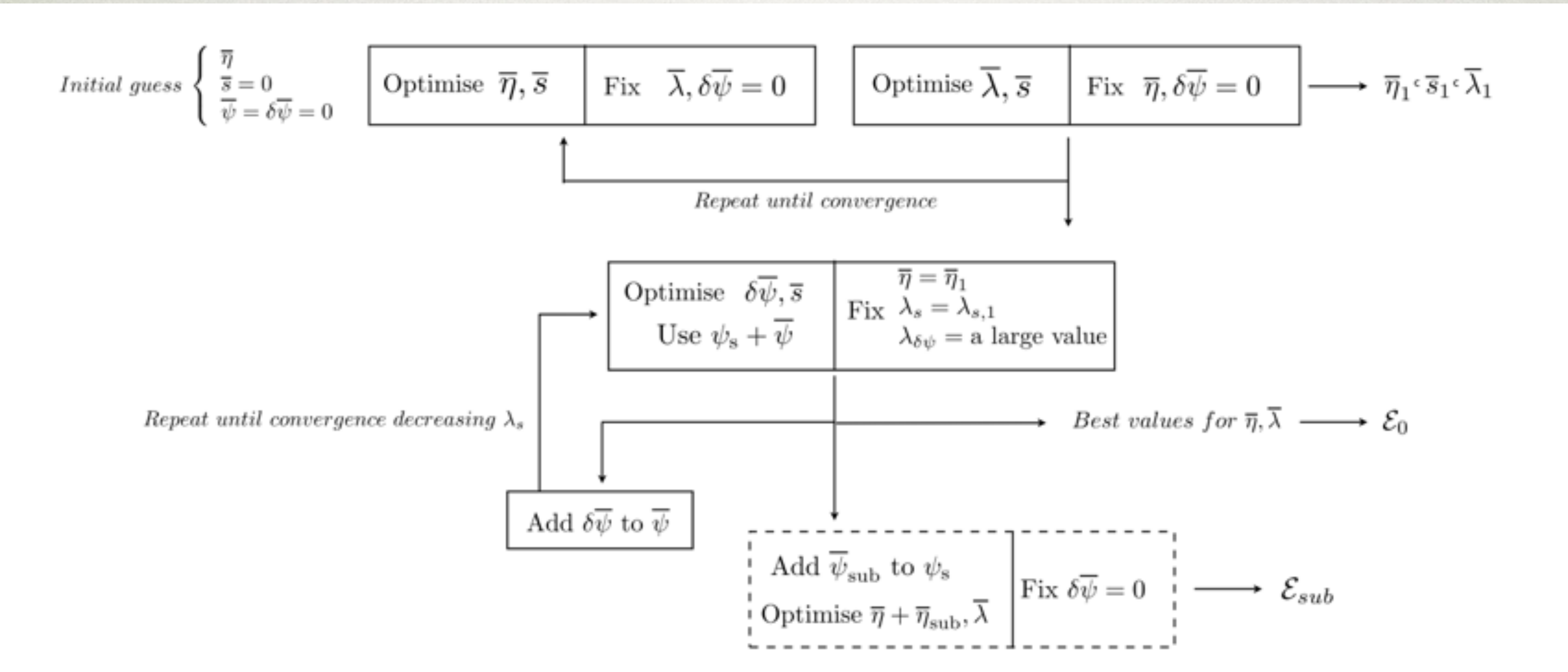

$$\kappa(x,y) = \frac{\kappa_0\left(2 - \frac{\gamma}{2}\right) q^{\gamma - 3/2}}{2(q^2(x^2 + r_c^2) + y^2)^{(\gamma-1)/2}}$$

$$\kappa(R) = \frac{\kappa_{0,\rm sub}}{2}\left[R^{-1} - (R^2 + r_t^2)^{-1/2}\right]$$

Gravitational Imaging

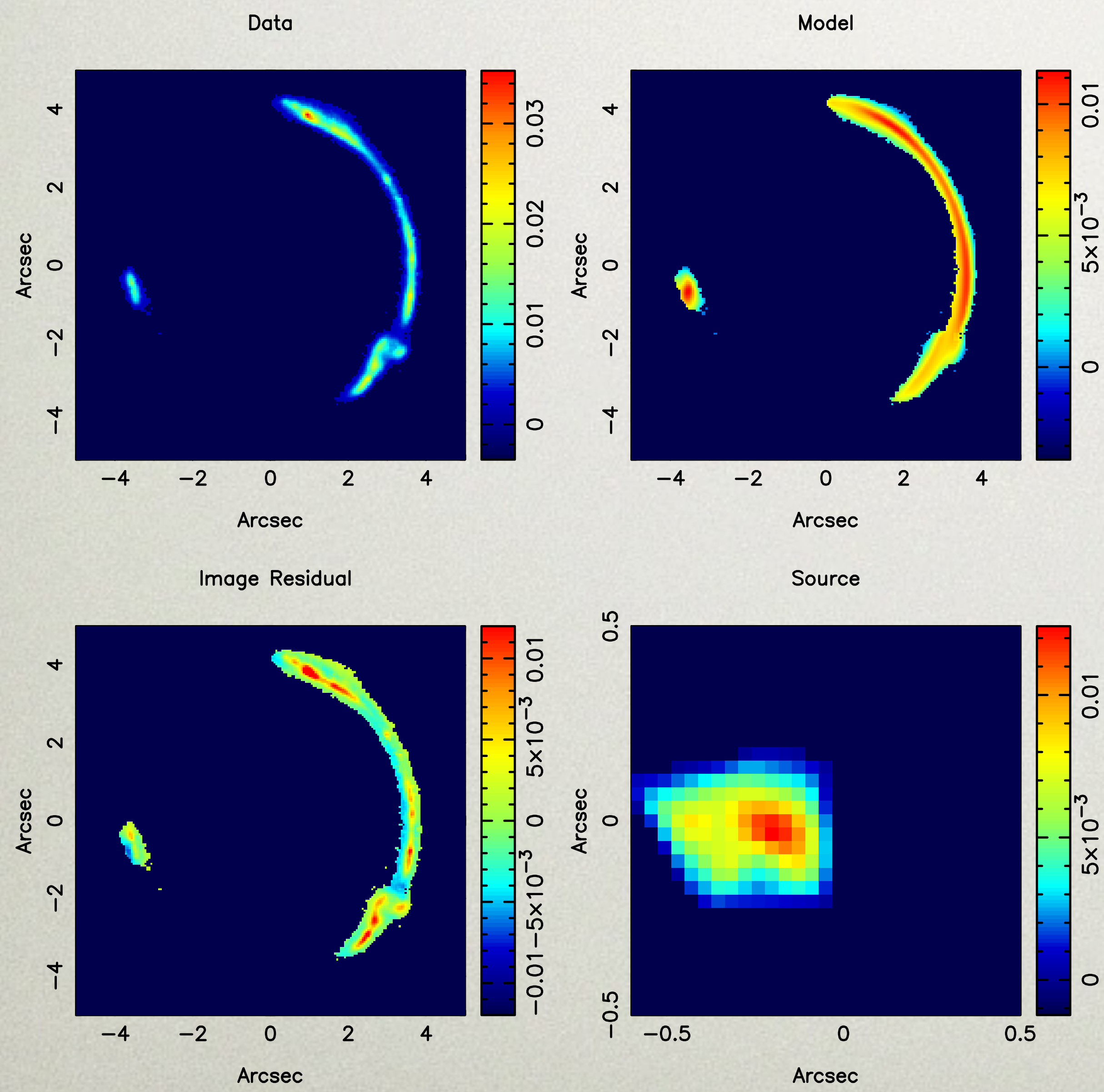

Simple smooth model with a power-law mass density profile

Gravitational Imaging

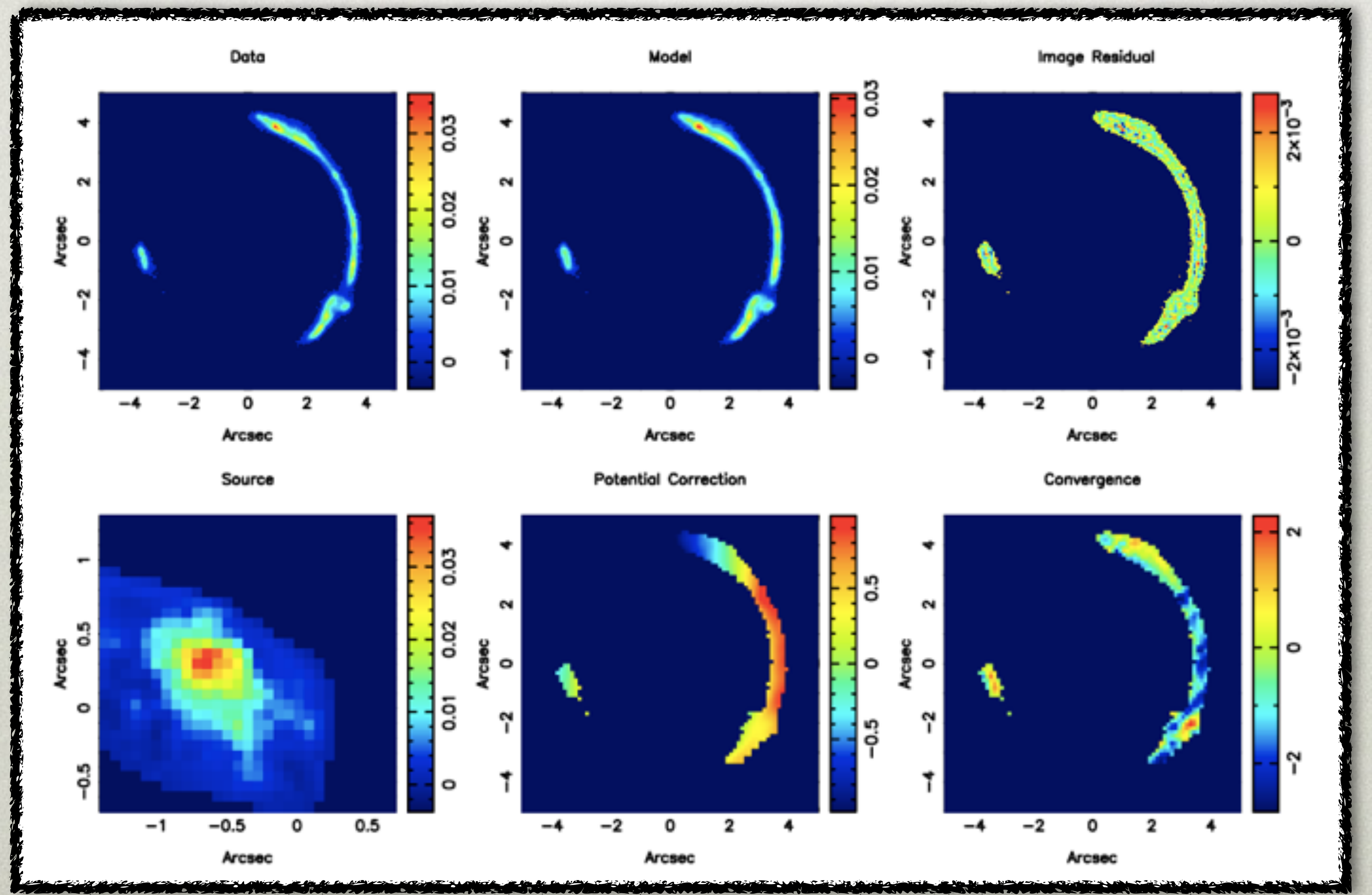

- Smooth model plus potential corrections

SLACS-Double ring

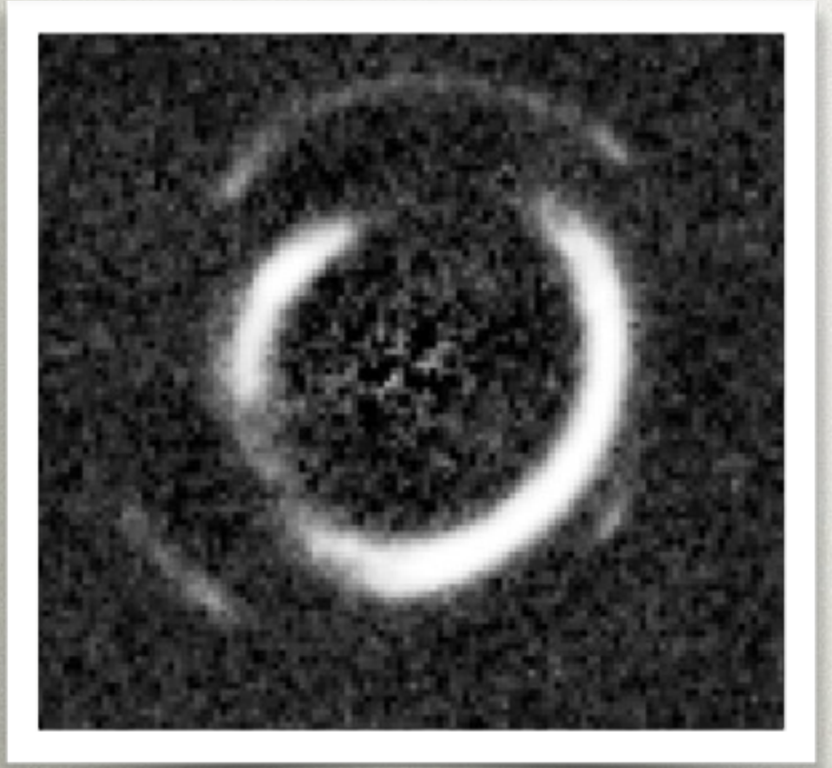

- Two concentric ring-like structures
- Dark-matter fraction: $f\,(< R_{eff}) = 73\% \pm 9\%$
- Expected number of mass substructure from CDM paradigm withi

$$\Delta R = R_{ein} \pm 0.3$$

- If f~5% (Dalal & Kochanek 2002), the expectation values for mass substructure is ~50 substructures

$$\mu(\alpha = 1.90, f = 0.3\%, R \in \Delta R) = 6.46 \pm 0.95$$

Double Ring

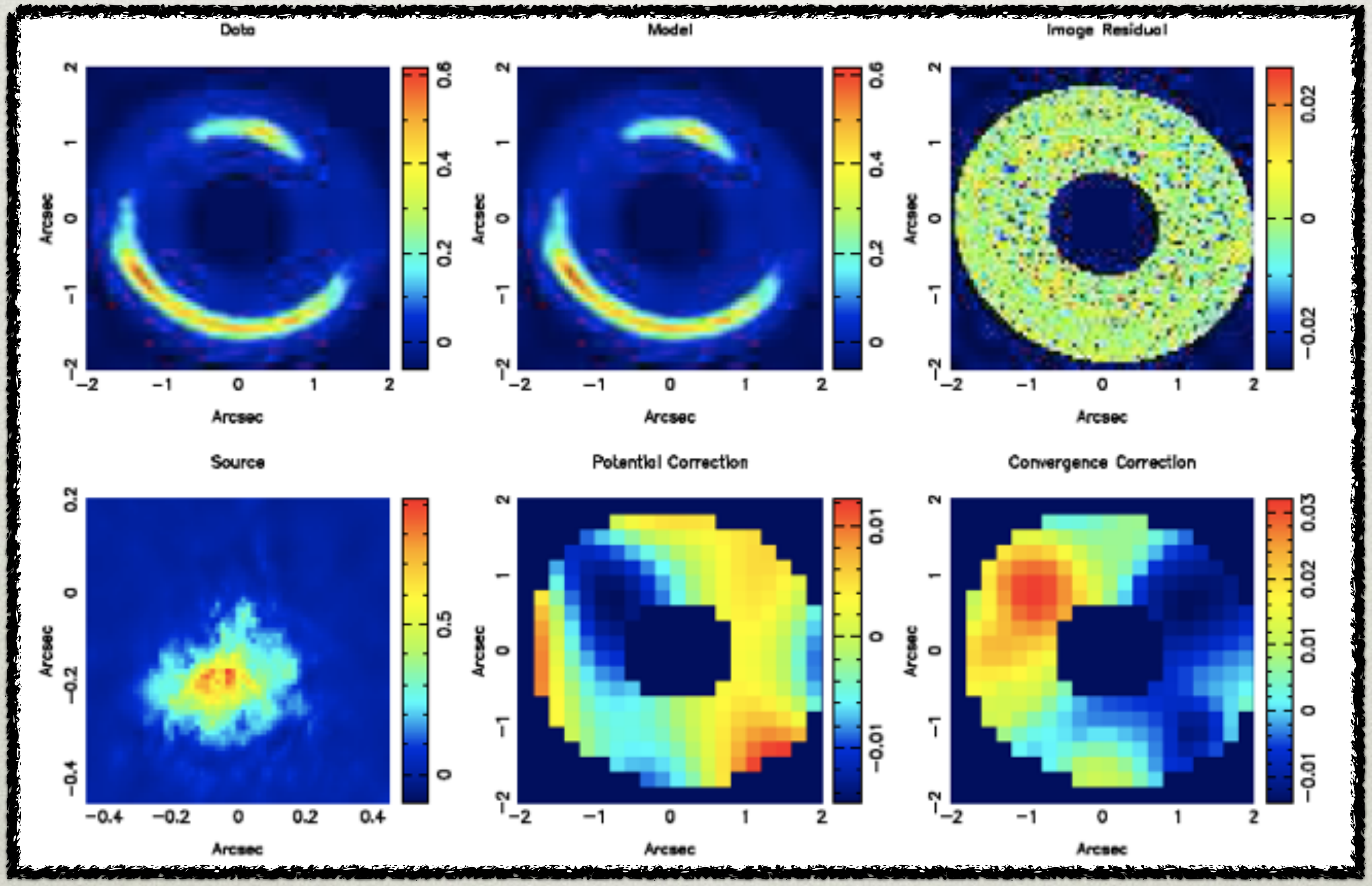

Results are stable against changes in the PSF, lens galaxy subtraction, pixel scale and rotation

Double Ring

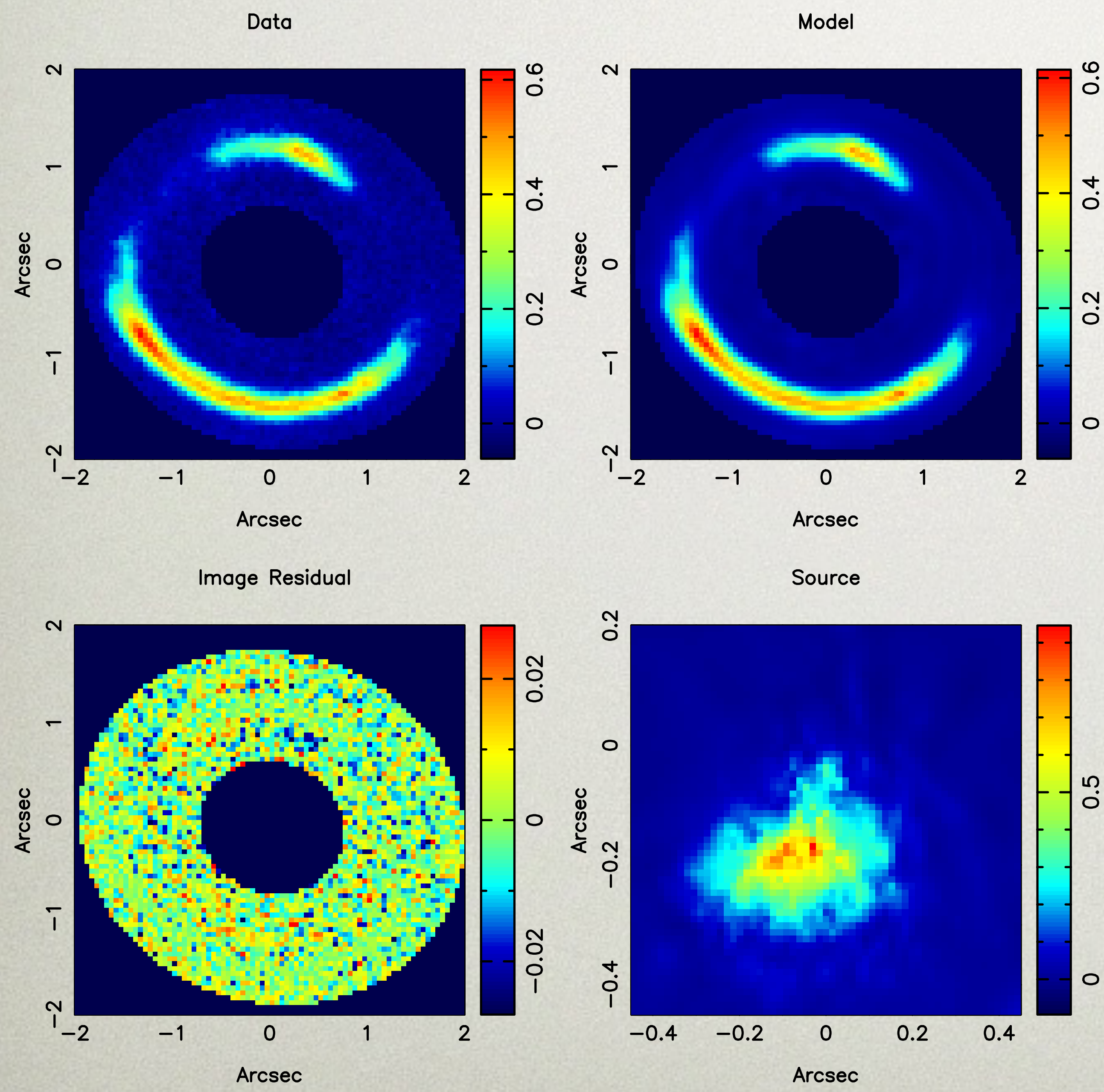

$$M_{\rm sub} = (3.51 \pm 0.15) \times 10^9 M_\odot$$

$$r_t = 1.1 \ kpc$$

$$\boxed{\Delta \log \mathcal{E} = -128.0}$$

$$L_V \leq 5 \times 10^6 L_\odot$$

$$M_{\rm 3D}(< 0.3) = 5.83 \times 10^8 M_\odot$$

$$({\rm M/L})_{\rm V,\odot} \geq 120 \ M_\odot/{\rm L}_{\rm V,\odot}$$

$z = 0.06 - 0.36 \quad \sigma_{\star} = 175 - 400 \; km \; s^{-1}$

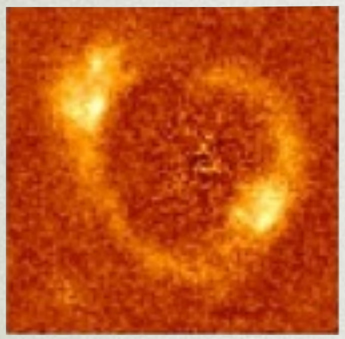

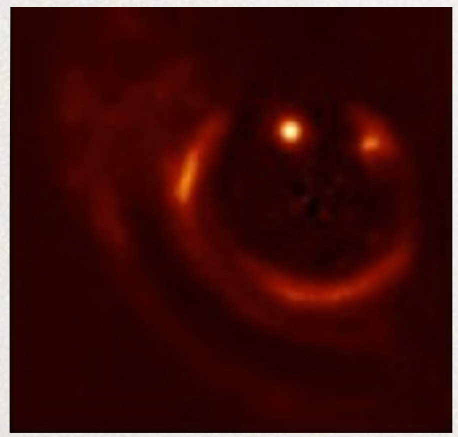

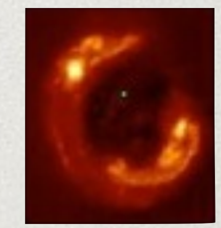

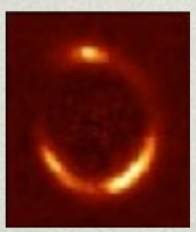

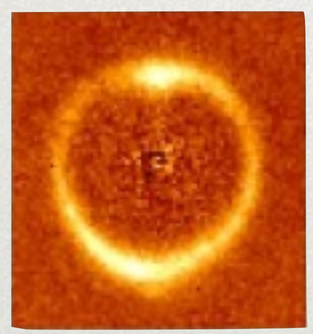

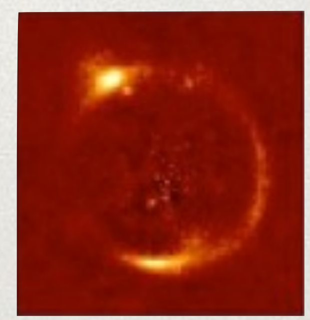

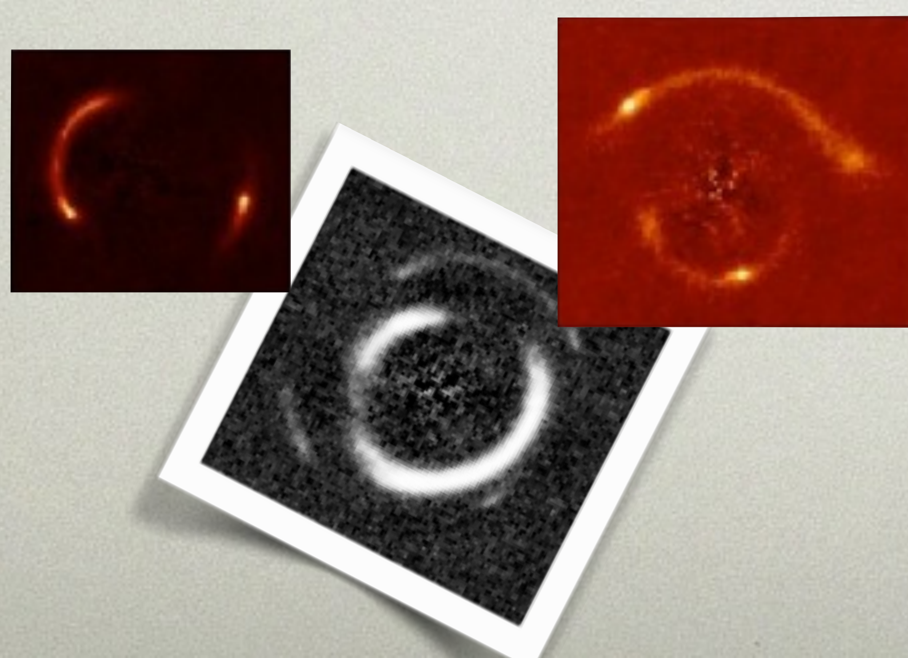

- Chosen on a s/n basis
- Representative sub-sample of the SLACS lenses
- Representative sample of massive early-type galaxies

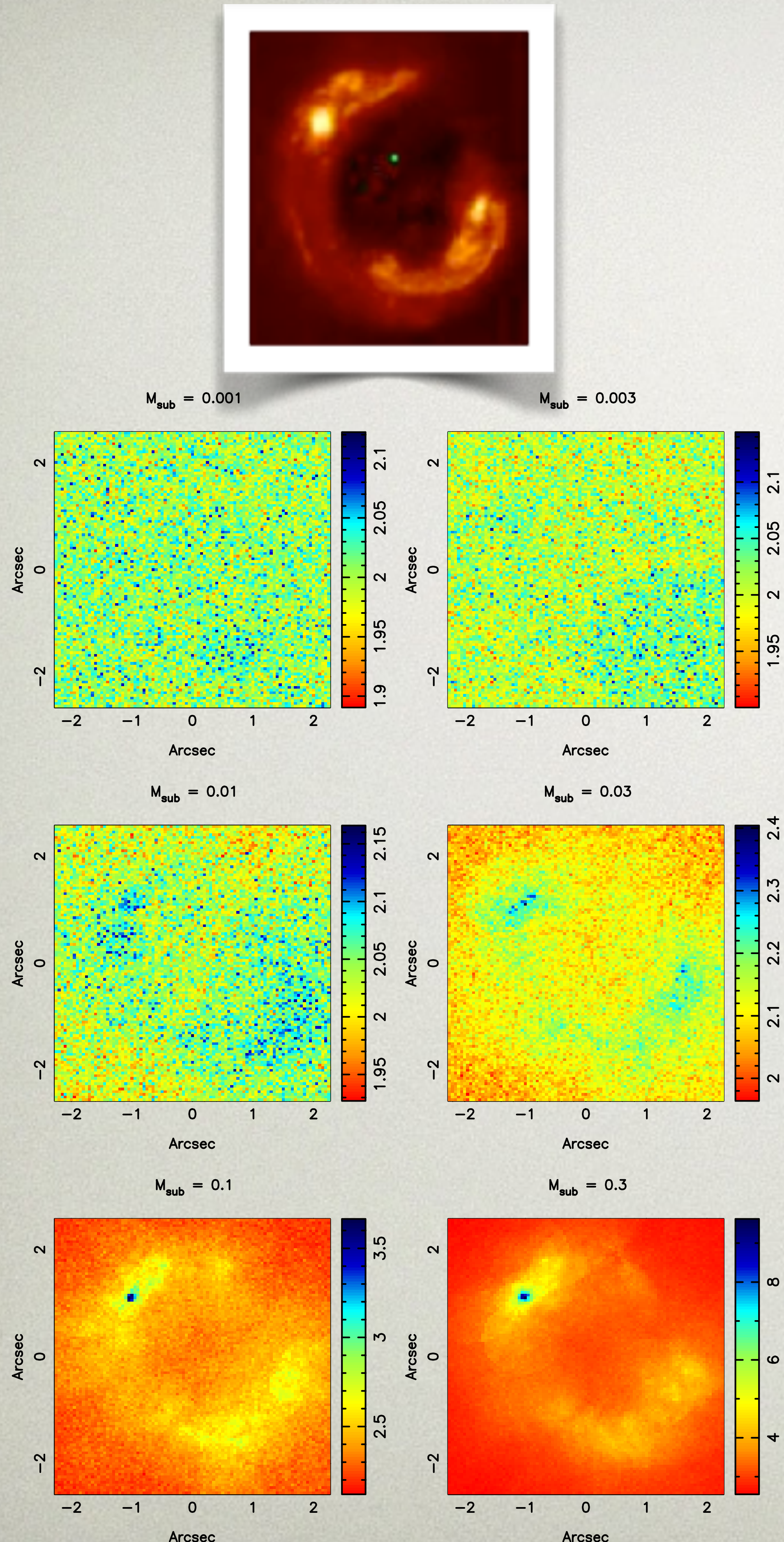

Msub = 0.001
Msub = 0.003
Msub = 0.01
Msub = 0.03
Msub = 0.1
Msub = 0.3
Arcsec

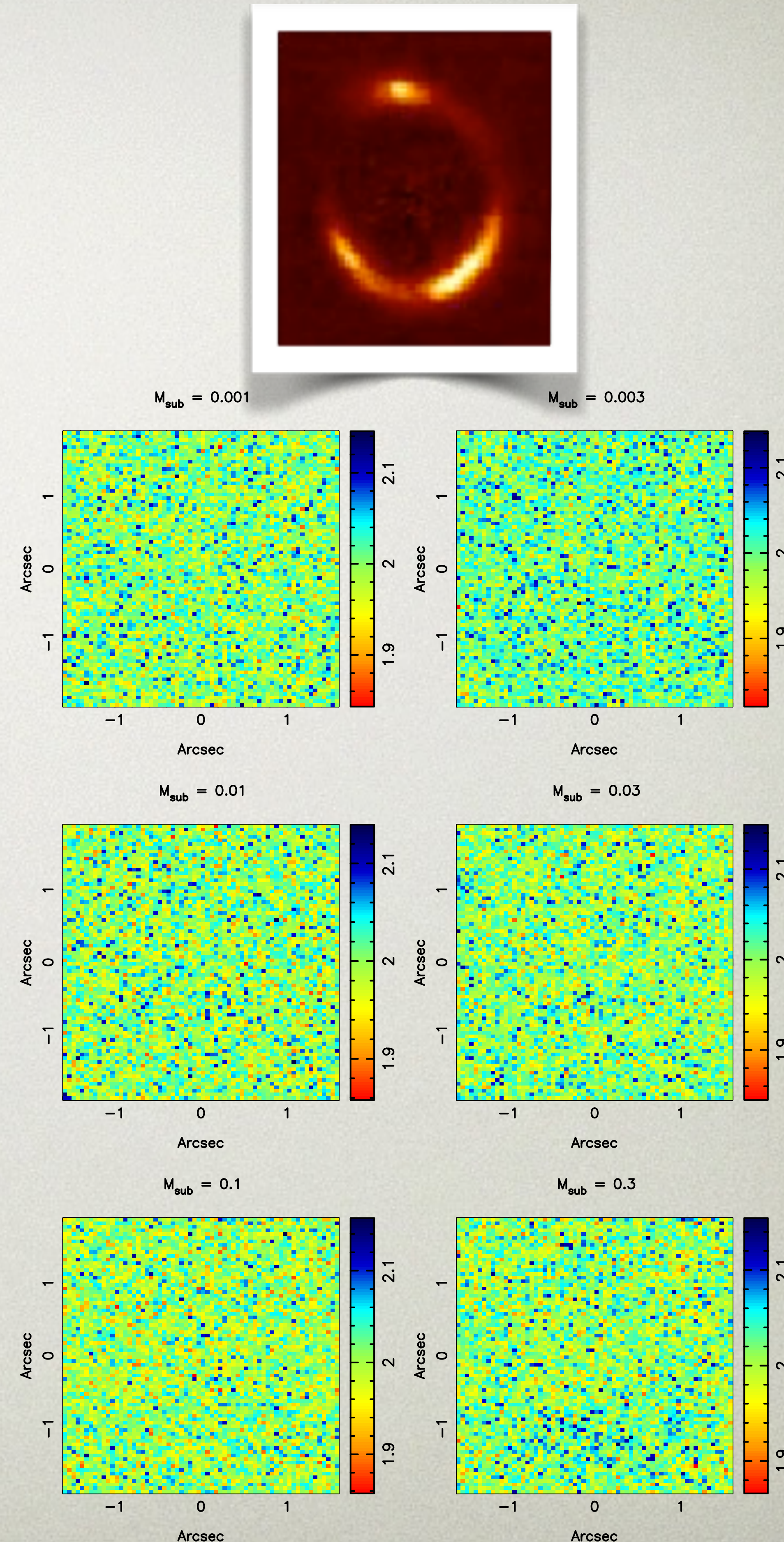

Msub = 0.001
Msub = 0.003
Msub = 0.01
Msub = 0.03
Msub = 0.1
Msub = 0.3
Arcsec

Sensitivity Function

$$\delta I \approx \nabla S \cdot \nabla \delta\psi = \nabla S \cdot \alpha_{sub}$$

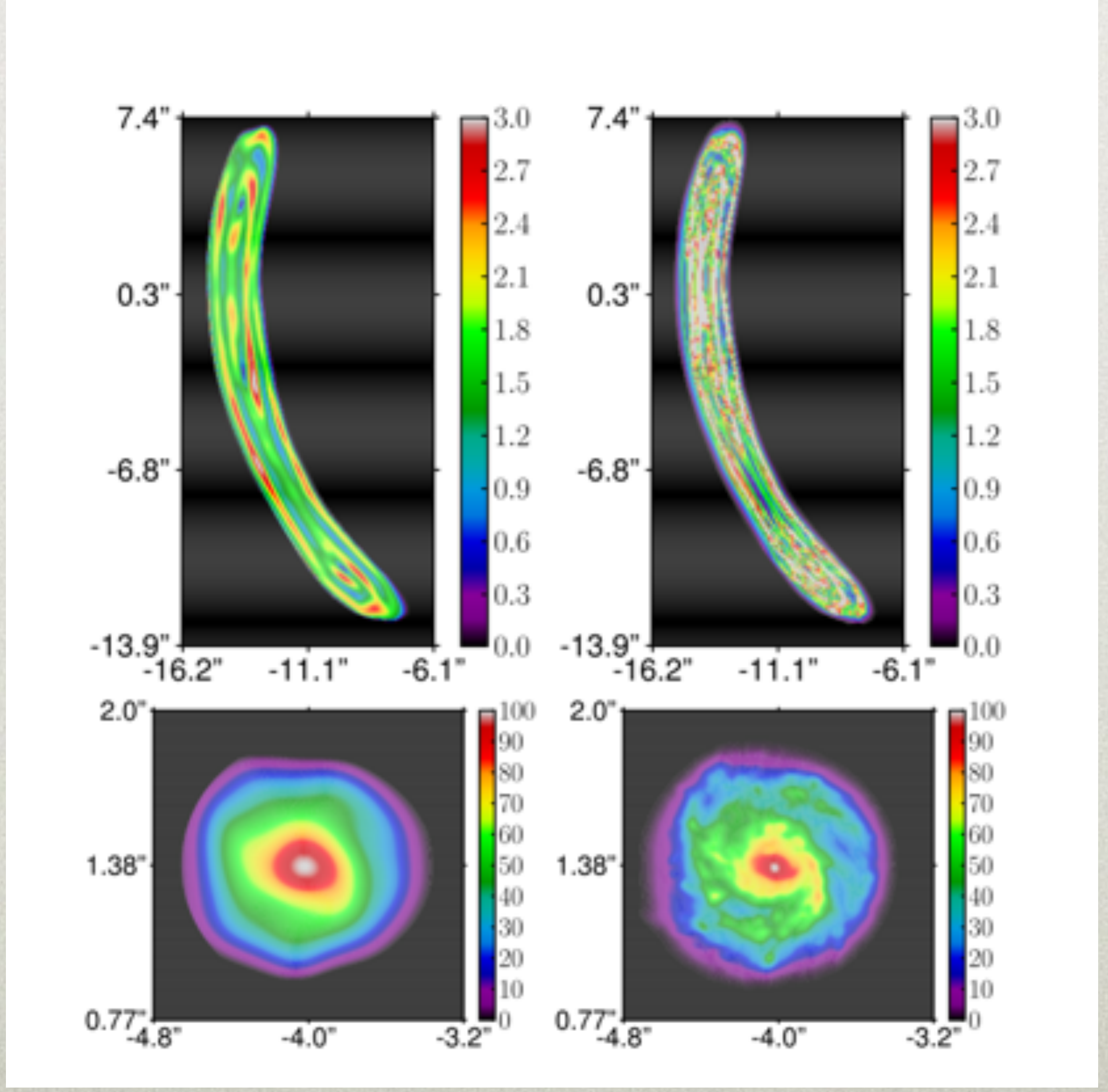

Likelihood

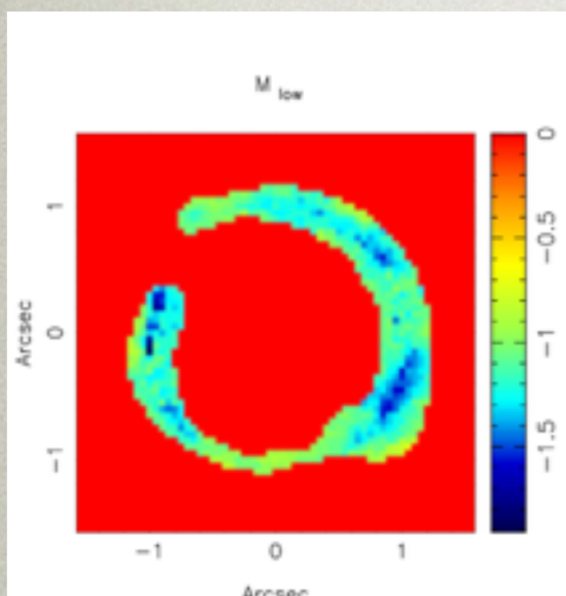

$$L\left(\{n_s, \mathbf{m_s}, \mathbf{R_s}\} \mid \alpha, f(<R), \mathbf{p}\right) = \frac{e^{-\mu(\alpha,f,\mathbf{p})}\ \mu(\alpha,f,\mathbf{p})^{n_s}}{n_s!} \prod_{k=1}^{n_s} P\left(m_k, R_k \mid \mathbf{p}, \alpha\right)$$

$$\mu_j(\alpha,f,\mathbf{p}) = \mu_{0,j}(\alpha,f,\mathbf{p}) \int_{M_{\mathrm{low,j}}}^{M_{\mathrm{max}}} P\left(m, R_j \mid \mathbf{p}, \alpha\right) dm$$

$$= \mu_{0,j}(\alpha,f,\mathbf{p}) \int_{M_{\mathrm{low,j}}}^{M_{\mathrm{max}}} \frac{dP}{dm}\ dm$$

$$\begin{cases} \mu_{0,j}(\alpha,f,\boldsymbol{p}) = \dfrac{f_j M_{\mathrm{DM}}(<R)}{\int_{M_{\mathrm{min}}}^{M_{\mathrm{max}}} m\ \frac{dP}{dm}\ dm} \\[2ex] f_j = \dfrac{f(<R)}{N_{\mathrm{pix}}} \end{cases}$$

$$\frac{dP}{dm} = \begin{cases} \dfrac{(1-\alpha)\ m^{-\alpha}}{\left(M_{\mathrm{max}}^{1-\alpha} - M_{\mathrm{min}}^{1-\alpha}\right)} & \alpha \neq 1 \\[2ex] \dfrac{m^{-\alpha}}{\ln\left(M_{\mathrm{max}}/M_{\mathrm{min}}\right)} & \alpha = 1 \end{cases}$$

Likelihood

$$L\left(\{n_s, \mathbf{m_s}, \mathbf{R_s}\} \mid \alpha, f(< R), \mathbf{p}\right) = \frac{e^{-\mu(\alpha,f,\mathbf{p})}\ \mu(\alpha, f, \mathbf{p})^{n_s}}{n_s!} \prod_{k=1}^{n_s} P\left(m_k, R_k \mid \mathbf{p}, \alpha\right)$$

$$P(m_k, R_k|\mathbf{p}, \alpha) = P(m_k|m)\, P(m|\alpha)\, P(R_k|r)P(r)$$

$$P\left(m_k, R_k \mid \boldsymbol{p}, \alpha\right) = \frac{\int_{M_{\rm low,k}}^{M_{\max}} \int_{R_k}^{r_{\max}} \mathcal{N}(m_k, \sigma_{m_k}|m_e) m^{-\alpha} P(R|r) P(r)\ dm\ dr}{\int_{M_{\min}}^{M_{\max}} \int_{R_k}^{r_{\max}} \mathcal{N}(m_k, \sigma_{m_k}|m_e) m^{-\alpha} P(R|r) P(r)\ dm\ dr}$$

$$P(R_k|r) = \frac{1}{r\sqrt{r^2/R_k^2 - 1}}$$

CDM Mass Function at z=0.2

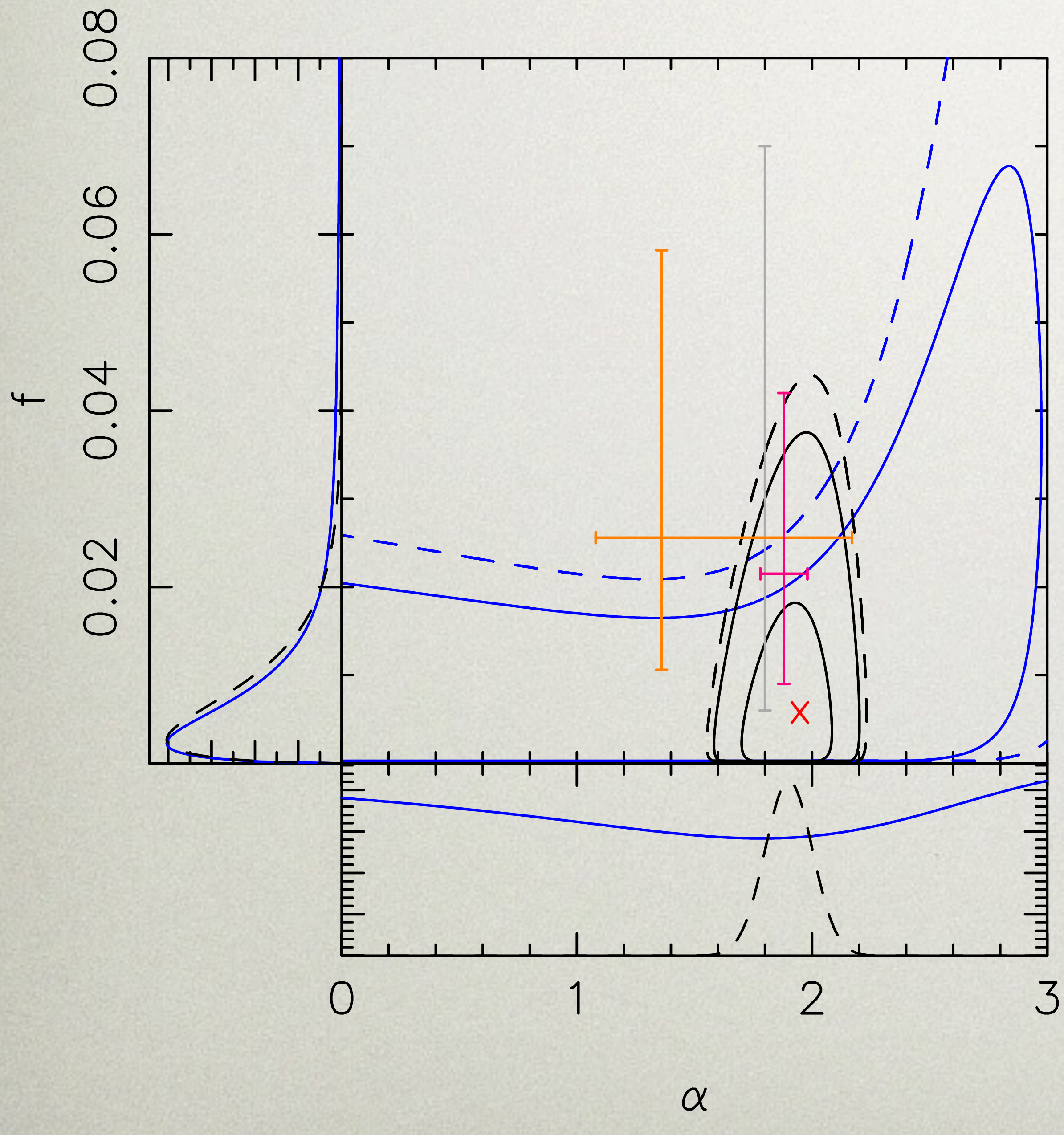

P(α)	f (68% CL)	α	ln Ev
U	$0.0076^{+0.0208}_{-0.0052}$	< 2.93 (95% CL)	-5.98
G	$0.0064^{+0.0080}_{-0.0042}$	$1.90^{+0.098}_{-0.098}$ (68% CL)	-6.13

SHARP

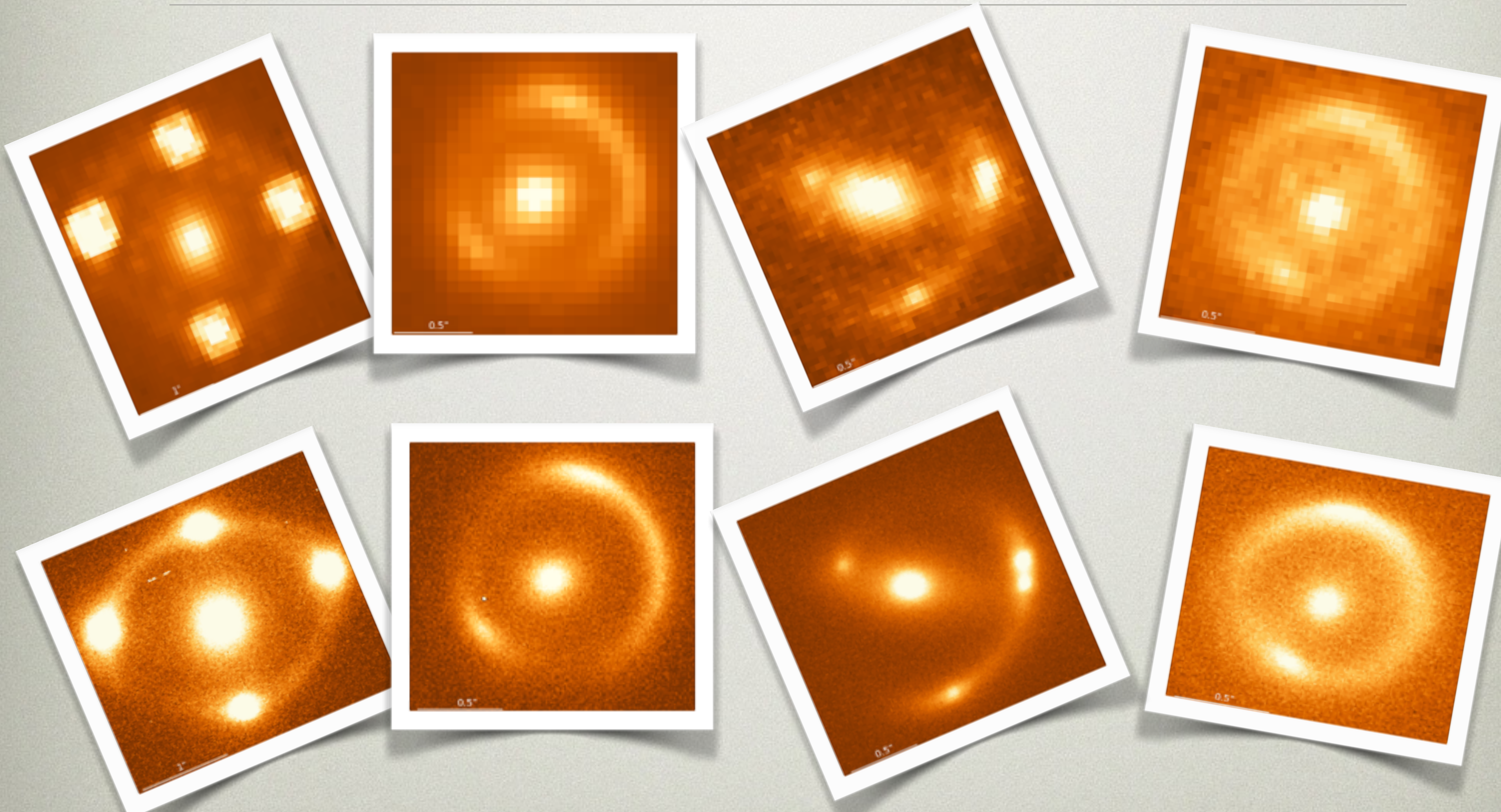

$$M_{low} = 10^8\ M_\odot$$

SHARP

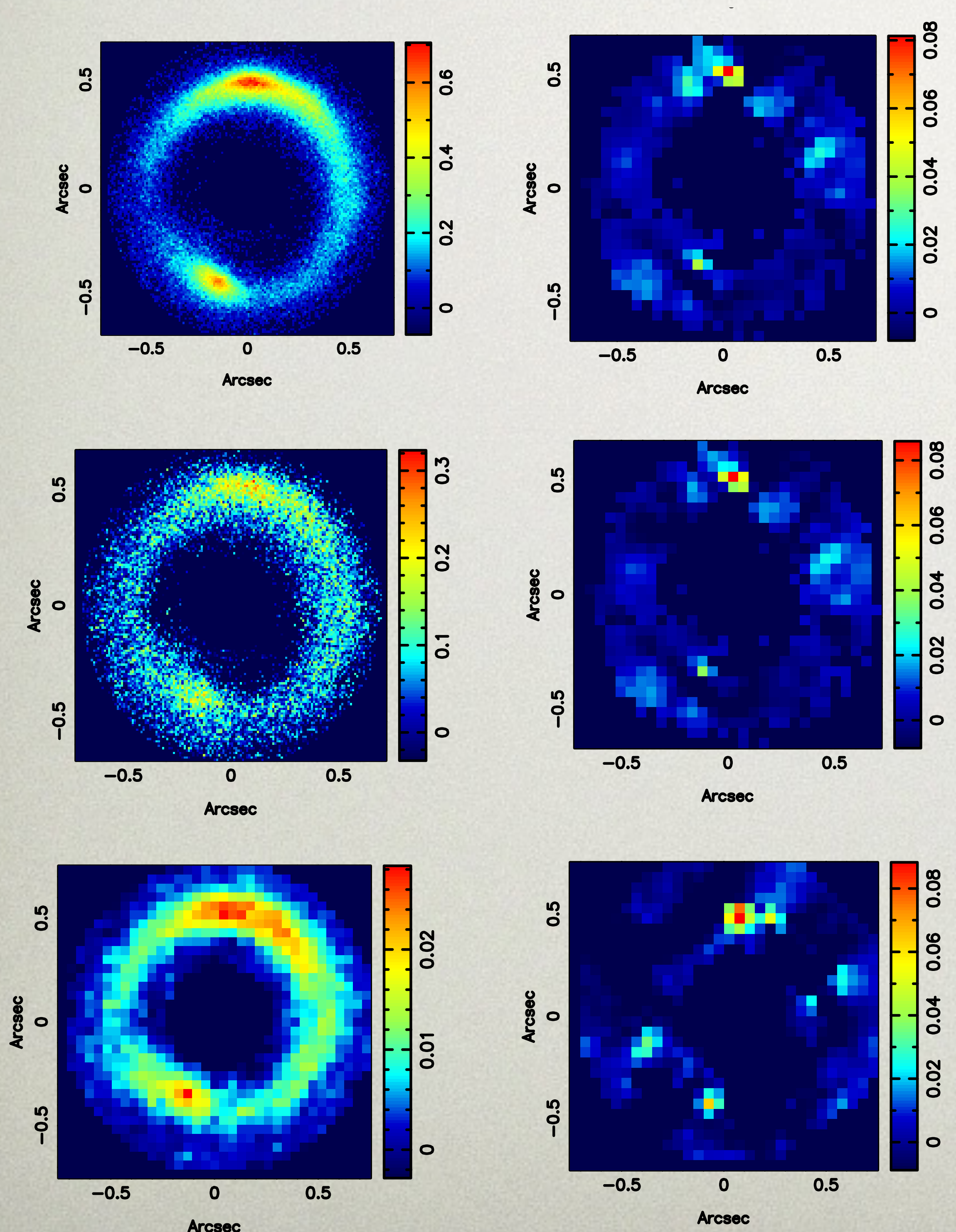

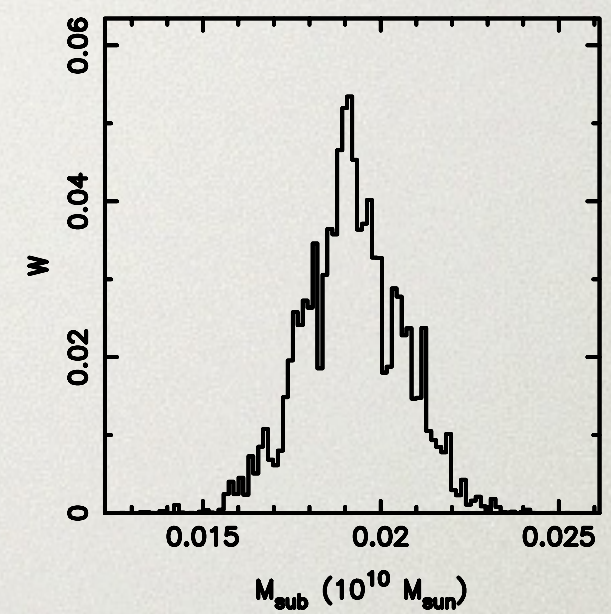

$$M_{sub} = (1.9 \pm 0.1) \times 10^{8} M_{\odot}$$

$$M(<0.6) = (1.15 \pm 0.06) \times 10^{8} M_{\odot}$$

$$M(<0.3) = (7.24 \pm 0.6) \times 10^{7} M_{\odot}$$

$$V_{max} \approx 27\ km\ s^{-1}$$

Radio - SHARP

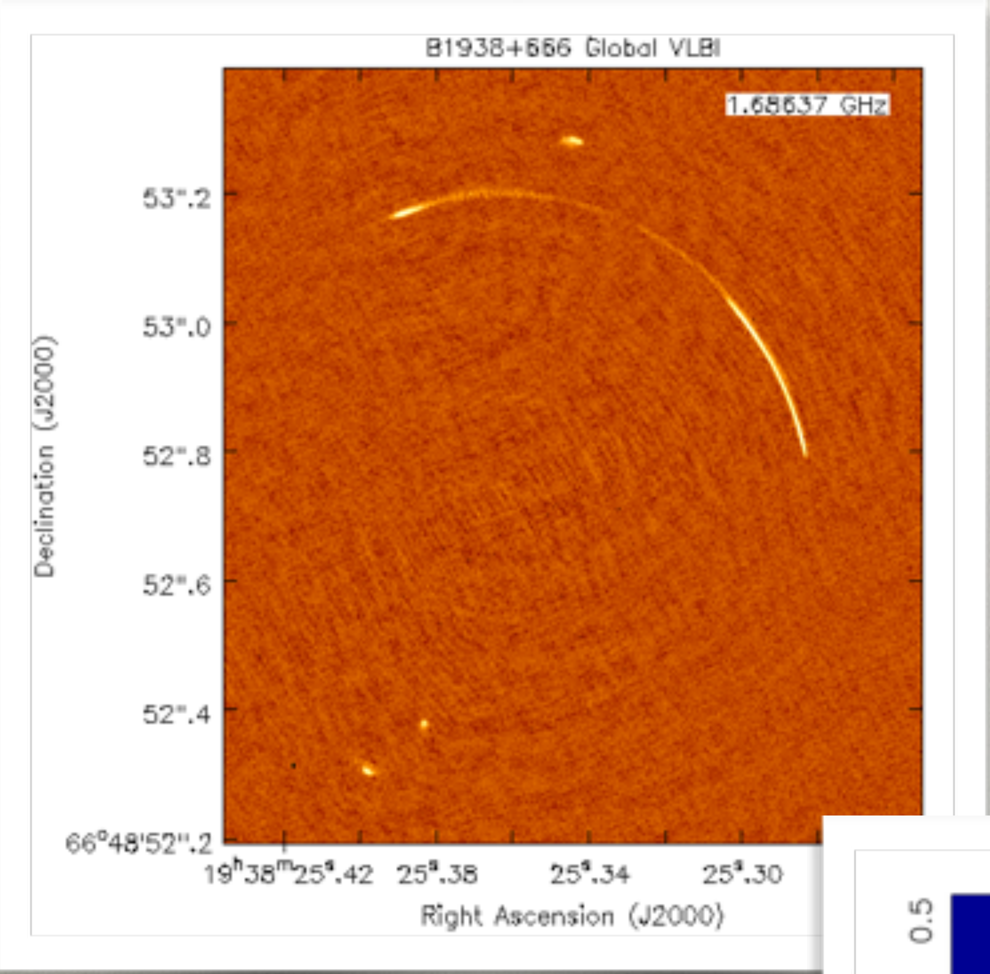
B1938+666 Global VLBI
1.68637 GHz
53".2
53".0
52".8
52".6
52".4
66°48'52".2
Declination (J2000)
19h38m25s.42
25s.38
25s.34
25s.30
Right Ascension (J2000)

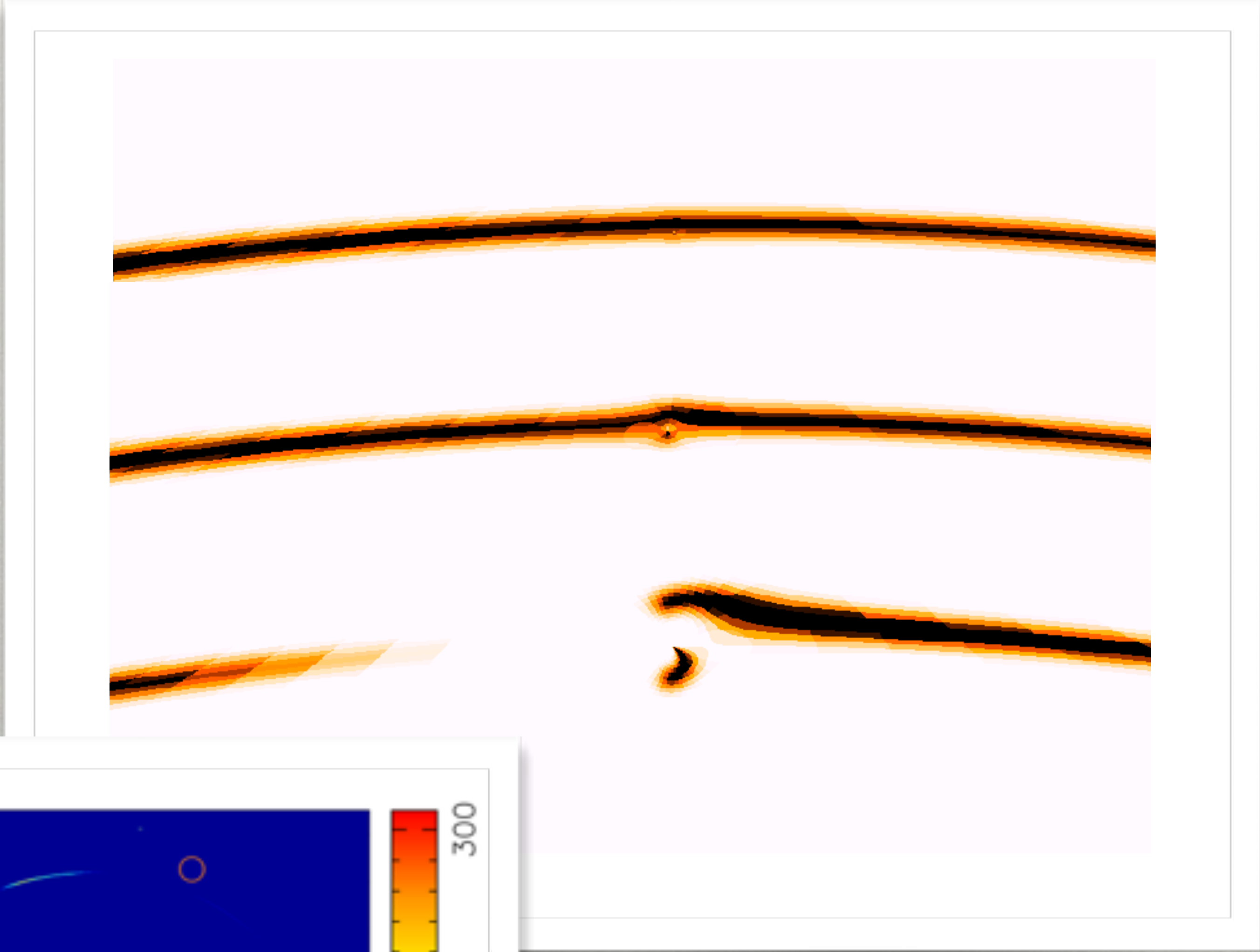

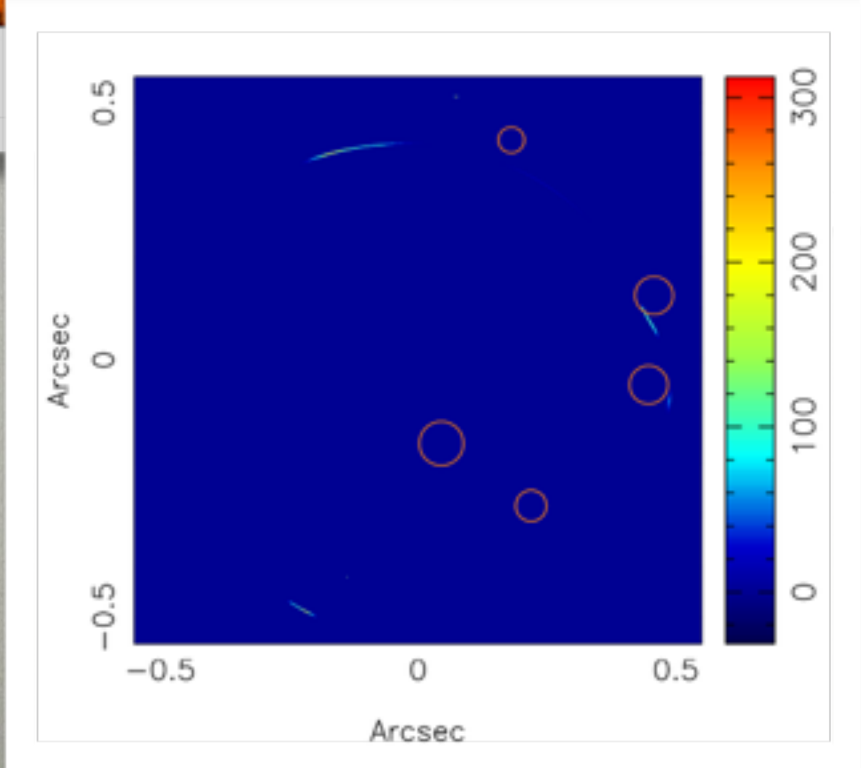
0.5
0
−0.5
Arcsec
−0.5
0
0.5
Arcsec
300
200
100
0

Conclusions

- Measuring the substructure mass function is an important test of the LCDM paradigm.
- The substructure mass function provides constraints on the dark matter properties
- Although most of the substructure could be dark or very faint gravitational lensing provides a great tool to probe the low mass end of substructure mass function
- Current results based on HST observations are in agreement with expectation from numerical simulation at masses ~ 10^8 M_sun